Performance Evaluation of Filtered Orthogonal Frequency Division Multiplexing (F-OFDM) in the Presence of Nonlinear Power Amplifier

A thesis submitted to the
Graduate School of Natural and Applied Sciences

by

Nann Win Moe Thet

in partial fulfillment for the
degree of Master of Science

in

Electronics and Computer Engineering

İSTANBUL
ŞEHİR
UNIVERSITY

This is to certify that we have read this thesis and that in our opinion it is fully adequate, in scope and quality, as a thesis for the degree of Master of Science in Electronics and Computer Engineering.

APPROVED BY:

Assist. Prof. Mehmet Kemal Özdemir (Thesis Advisor) .....

Assist. Prof. Hakan Doğan .....

Assoc. Prof. Tansal Güçlüoğlu .....

This is to confirm that this thesis complies with all the standards set by the Graduate School of Natural and Applied Sciences of İstanbul Şehir University:

DATE OF APPROVAL: 06.09.2017

SEAL/SIGNATURE:

Declaration of Authorship

I, Nann Win Moe Thet, declare that this thesis titled, 'Performance Evaluation of Filtered Orthogonal Frequency Division Multiplexing (F-OFDM) in the Presence of Nonlinear Power Amplifier' and the work presented in it are my own. I confirm that:

- This work was done wholly or mainly while in candidature for a research degree at this University.
- Where any part of this thesis has previously been submitted for a degree or any other qualification at this University or any other institution, this has been clearly stated.
- Where I have consulted the published work of others, this is always clearly attributed.
- Where I have quoted from the work of others, the source is always given. With the exception of such quotations, this thesis is entirely my own work.
- I have acknowledged all main sources of help.
- Where the thesis is based on work done by myself jointly with others, I have made clear exactly what was done by others and what I have contributed myself.

Signed: 

Date: 04/08/2017

Performance Evaluation of Filtered Orthogonal Frequency Division Multiplexing (F-OFDM) in the Presence of Nonlinear Power Amplifier

Nann Win Moe Thet

Abstract

Orthogonal Frequency Division Multiplexing (OFDM) has been a reliable modulation technique in 4G due to its ability to combat the intersymbol interference (ISI) caused by multipath channel and its efficient usage of spectrum due to orthogonality properties. However, OFDM as is faces challenges when it comes to supporting 5G applications requirements due to its high peak to average ratio (PAPR) and inability to provide asynchronous transmission. Therefore, filtered-OFDM (F-OFDM), which is the modified version of OFDM that separates the total assigned bandwidth into many sub-bands and then filtering each sub-band with an appropriate designed filter, was proposed in recent years. Many studies have been focusing on the performance of a F-OFDM system alone without taking the effect of power amplifier (PA) into account in the system. Therefore, in this thesis, we evaluate the performance of point-to-point F-OFDM system in the presence of nonlinear PA and also employ techniques used in OFDM system to reduce the effect of the PA. In this regard, we first simulate a basic F-OFDM system without a PA by using filters obtained from different filtering methods such as window based filter and Parks-McClellan filter. Specifically, the performance analysis is done in terms of power spectral density (PSD) and bit error rate (BER). Secondly, the performance of F-OFDM system with a nonlinear PA is analyzed, and it is observed that the out-of-band (OOB) emission is increased as expected. Hence, pre-distortion is also included in the system to linearize the response of the PA. From the simulation results, it is seen that OOB spectrum regrowth due to the PA is suppressed fully, yet it does not reach to the original OOB emission level. Lastly, a modified version of optimized iterative clipping and filtering (ICF) is introduced to optimize the high PAPR of the f-OFDM signal. With the optimized ICF method, the PAPR is greatly reduced, resulting in lower OOB emission. With the combination of optimized ICF and pre-distortion, the overall performance of F-OFDM system in the presence of nonlinear PA is improved compared to the system without a pre-distorter.

Keywords: 5G, F-OFDM, filter, PA, OOB, DPD, Optimized ICF

Doğrusal Olmayan Güç Amplifikatörü Varlığında Filtrelenmiş Ortogonallık Frekans Bölmeli çoğullama-OFDM'nin Performans Değerlendirmesi

Nann Win Moe Thet

Öz

Orthogonal Frequency Division Multiplexing (OFDM), çok kanallı kanalın neden olduğu intersymbol enterferans (ISI) ve diklik özelliklerinden dolayı spektrumun verimli kullanımı nedeniyle 4G'de güvenilir bir modülasyon tekniğidir. Bununla birlikte, OFDM, yüksek tepe ortalam oranına (PAPR) ve eşzamansız iletim sağlanamamasına bağlı olarak 5G uygulamaları gereksinimlerini destekleme konusunda zorluklarla karşı karşıyadır. Bu nedenle, toplam atanmış bant genişliğini birçok alt-banda ayıran ve daha sonra her bir alt bandı uygun tasarlanmış bir filtre ile filtreleyen OFDM'nin değiştirilmiş hali olan filtrelenmiş-OFDM (F-OFDM) son yıllarda önerilmiştir. Birçok çalışma, sistemde güç yükselticisinin (PA) etkisini dikkate almadan tek başına bir F-OFDM sisteminin performansına odaklanıyor. Bu nedenle, bu tezde doğrusal olmayan PA varlığında noktadan noktaya F-OFDM sisteminin performansını ve OFDM sisteminde PA'nın etkisini azaltmak için kullanılan teknikleri de değerlendiriyoruz. Bu bağlamda, önce pencere tabanlı filtre ve Parks-McClellan filtresi gibi farklı filtreleme yöntemlerinden elde edilen filtreleri kullanarak PA içermeyen basit bir F-OFDM sistemini simüle ediyoruz. Spesifik olarak, performans analizini güç spektrum yoğunluğu (PSD) ve bit hata oranı (BER) açısından yapıtık. İkincil olarak, doğrusal olmayan bir PA ile F-OFDM sisteminin performansı analiz edildi ve bant dışı (OOB) emisyonunun beklendiği gibi arttığı gözlendi. Bu nedenle, PA'nın tepkisini doğrusallaştırmak için ön bozulma da sisteme dahil edildi. Simülasyon sonuçlarına göre, PA nedeniyle OOB tayfının yeniden büyümesinin tamamen bastırıldığı, ancak orijinal OOB emisyon seviyesine ulaşılmadığı görülmektedir. Son olarak, F-OFDM sinyalinin yüksek PAPR'sini optimize etmek için, optimize yinelemeli kırpma ve filtreleme (ICF) yaklaşımının modifiye edilmiş bir versiyonu sunulmuştur. Optimize edilmiş ICF yöntemi ile PAPR büyük ölçüde azaltılmış ve OOB emisyonu düşürülmüştür. Bu şekilde optimize edilmiş ICF ve ön bozulma kombinasyonu ile lineer olmayan PA varlığında F-OFDM sisteminin genel performansı, ön distorter içermeyen sisteme kıyasla geliştirildi.

Anahtar Sözcükler: 5G, F-OFDM, filtre, PA, OOB, DPD, Optimize ICF

To my parents and my sister and brothers

Acknowledgments

First and foremost, I would like to express my gratitude to my advisor Prof. Kemal Özdemir for his valuable guidance during my MSc. studies, for his support, patience, motivation and broad knowledge. His guidance assisted me a lot in my research and the completion of the thesis. Without his endless support and patience, this thesis will never be completed.

I would also like to thank my thesis committee, Assist. Prof. Hakan Doğan and Assoc. Prof. Tansal Güçlüoğlu, for their thorough evaluation and helpful comments.

I greatly would like to thank and acknowledge the graduate scholarship (TÜBİTAK 2215) supported by TÜBİTAK BİDEB. Because of the financial help from TÜBİTAK, I was able to complete my study in Turkey without any worry.

Also, I would like to thank my fellow graduate students and friends for their helps, advice, and understandings throughout my study here.

Last but not the least, I would like to thank my parents, sister and brothers for their consistent support and encouragement. Without their love and support, I would not be where I am now.

Contents

List of Figures

Abbreviations

OFDM	**O**rthogonal **F**requency **D**ivision **M**ultiplexing
F-OFDM	**F**iltered **OFDM**
F-OFDMA	**F**iltered **O**rthogonal **F**requency **D**ivision **M**ultiple **A**ccess
f-DFT-S-OFDMA	**f**iltered **D**iscrete **F**ourier **T**ransform **s**pread OFDMA
W-OFDM	**W**indowing **OFDM**
ISI	**I**ntersymbol **S**ymbol **I**nterference
PA	**P**ower **A**mplifier
HPA	**H**igh **P**ower **A**mplifier
PSD	**P**ower **S**pectrum **D**ensisty
BER	**B**it **E**rror **R**ate
OOB	**O**utg **O**f **B**and
ICF	**I**terative **C**lipping and filtering
FDMA	**F**requency **D**ivision **M**ultiple **A**ccess
GSM	**G**lobal **S**ystem for **M**obile communication
TDMA	**T**ime **D**ivision **M**ultiple **A**ccess
CDMA	**C**ode **D**ivision **M**ultiple **A**ccess
GPRS	**G**eneral **P**acket **R**adio **S**ervice
LTE	**L**ong **T**erm **E**volution
QoS	**Q**uality **o**f **S**ervice
MIMO	**M**ultiple **I**nput **M**ultiple **O**utput
IoT	**I**nternet **o**f **T**hings
3GPP	**3**rd **G**eneration **P**artnership **P**roject
mMTC	**m**assive **M**achine **T**ype **C**ommunications
URLLC	**U**ltra **R**eliable **L**ow **L**atency **C**ommunications
eMBB	**E**nhanced **M**obile **B**road**B**and
IMT	**I**nternational **M**obile **T**elecommunications

TTI	**T**ransmission **T**ime **I**nterval
V2V	**V**ehicle **t**o **V**ehicle communication
UF-OFDM	**U**niversal **f**iltered-**OFDM**
UFMC	**U**niversal **f**iltered **m**ulticarrier
ZP	**Z**ero **P**refix
CP	**C**yclic **P**refix
UEs	**U**ser **E**quipments
BS	**B**ase **S**tation
BLER	**BL**ock **E**rror **R**ate
FIR	**F**inite **I**mpulse **R**esponse
DPD	**D**igital **P**re**D**istortion
M-QAM	**M** order **Q**uadrature **A**mplitude **M**odulation
AWGN	**A**dditive **W**hite **G**aussian **N**oise
dB	**d**eci**B**al
TWT	**T**raveling **W**ave **T**ube
SSPA	**S**olid **S**tate **P**ower **A**mplifier
AM-AM	**AM**plitude to **AM**plitude
AM-PM	**AM**plitude to **P**hase
LTI	**L**inear **T**ime **I**nvariant
MP	**M**emory **P**olynomial
PAPR	**P**acket **E**rror **R**ate
EVM	**E**rror **V**ector **M**agnitude
SNR	**S**ignal **N**oise **R**atio
IFFT	**I**nverse **F**ast **F**ourier **T**ransform
FFT	**F**ast **F**ourier **T**ransform

Chapter 1

Introduction and Motivation

In this chapter, the development of wireless communication generations will be firstly presented. Then the filtered-OFDM, which is considered to be used in 5G, will be introduced. Lastly, motivation of this research will be elaborated.

1.1 Evolution of Wireless Communications

Communication technologies have been evolving from using fires, beacons, smoke signals, communication drums, horns, etc. to using digital signals today. Conveying information is quicker than ever with the advent of Internet. Thanks to telecommunication technologies nowadays, not only human beings but also smart devices, vehicles, robots etc. are communicating effectively and efficiently over a distance. As we manifest how often we need smart phones day to day, we can see communication is indispensable in our lives.

Back in the history, telegraph is the earliest invention of a wired electrical communications, which was introduced by Samuel Morse in 1837 with the aid of the electric battery invented by Alessandro Volta in 1799. The first transatlantic wire cable for telegraphy was installed in 1858 by linking between the United States and Europe, however, the operation was failed after four weeks. After the telegraphy invention, the era of telephony started in the 1870s. The invention of the first electric telephone by Alexander Graham Bell was patented in 1876, and Gardiner Greene Hubbard founded the Bell Telephone Company in 1877 [12]. In 1880, Graham Bell and Charles Sumner Tainter developed the first wireless telephone, known as photophone, which transmits voice over light waves

[13]. Their first transmission was conducted over 213 meters long distance. However, the photophone was easily affected by outdoor interference.

Later, an Italian inventor named Guglielmo Marconi developed a wireless telegraphy by improving the Hertz telegraphy system. He aimed to implement the wireless telegraphy in practice for very long distances without the need of wire, and in 1902, the first transatlantic radiotelegraphy transmission over the English Channel between England and Newfoundland was succeeded. Due to his long distance wireless telegraphy, the lives of many people in ship collisions were saved; Titanic survivors set one of the cases [14].

The development of wireless communications have been improving consistently since the beginning of the radio waves discovery. In the modern telecommunications era, the first generation (1G) of wireless mobile telecommunications technology, which can transmit the analog voice only, was introduced in the early 1980. There are different standards in 1G, and all of them uses Frequency Division Multiple Access (FDMA) technique, where users are separate from each other in frequency domain. One of the disadvantages of 1G is that it can only transmit analog signals, which does not have the ability to withstand channel interference. Therefore, the voice signals could be easily interrupted by noise [15, 16].

Besides, since encryption techniques used in 1G devices were not advanced yet, communication was not safe enough. The most inconvenient side of the 1G is that only mobile devices from the same network provider could communicate with each other, and handover between different base stations was not also allowed. A more serious issue was that it was relatively an easy task to clone the mobile terminals in 1G networks [15, 16].

Due to the limitations in 1G, second generation (2G) was developed in early 1990s. In 2G, which is based on the Global System for Mobile communication (GSM) technology, data is transmitted in digitized form unlike 1G, and in addition to the voice signals, text messaging, voice-mail and simple emails are also offered. Due to the digital transmission system, the voice signal quality is improved and better data security was also provided. With Time Division Multiple Access (TDMA), which separates users in time domain; and Code Division Multiple Access (CDMA), which can support more users with its large spectrum capacity, 2G was able to provide transmission rate up to 64 kbps [15][16].

Even though TDMA can provide richer services with higher data rates, there were connection problems on the user when they were moving. In TDMA technology, each user has its own time slot to transmit data. When the user moves from one cell region to another, connection can be dropped if there is no available time slot in the cell anymore. 2G can supply better data rates compared to 1G, however, with the needs of transmission for multimedia data such as image, audio, and video, much higher data rates were in demand, which lead to the advancement of 2.5G. 2.5G uses the General Packet Radio Service (GPRS) technology, which can provide transmission speed up to 144 kbps. The new features of the 2.5G includes multimedia messaging and Internet services such as web browsing and emails. [15][16]

Transmission rate achieved in this generation is never enough to catch up the required rate of the more advanced services. In the 2000s, 3G was developed in the demand of faster data transmission with the development of smart phones. Some of the features in 3G are swift mobile internet access, global roaming, video streaming, video conferencing, and 3D game. It also allows faster web browsing and large email service with the data speed up to 2Mpbs. The faster mobile services of 3G were realized with the combination technique of CDMA and TDMA. However, theses services of the 3G were expensive and also more spectrum bandwidth were required to supply more services. Moreover, while moving at the high speed, data rate of 3G is reduced to very low rate of 145 kbps [15], [16].

In every generation in wireless communications, data transmission rate is always high and hence improvements are needed. This, on the other hand, forced us to come up with a new technology in every decade. In the late 2000s, 4G was evolved with the enhanced technology of 3G, which is know as Long Term Evolution (LTE). Unlike 3G , which uses hybrid voice and data networks, in LTE, data-only Internet Protocol (IP) network is considered. The additional feature in 4G is Quality of Service (QoS), which prioritizes the internet data traffic to allocate more bandwidth to the most important services or applications. Moreover, with the help of the technology such as OFDM (Orthogonal frequency-division multiplexing) and MIMO (multiple input, multiple output), 4G can provide larger coverage, larger bandwidth (about 20 MHz), more users in the same available bandwidth and higher data rate in the range of 100 Mbps up to 1 Gbps. The summary of the development of wireless communications from 1G up to 4G is illustrated in Figure 1.1.

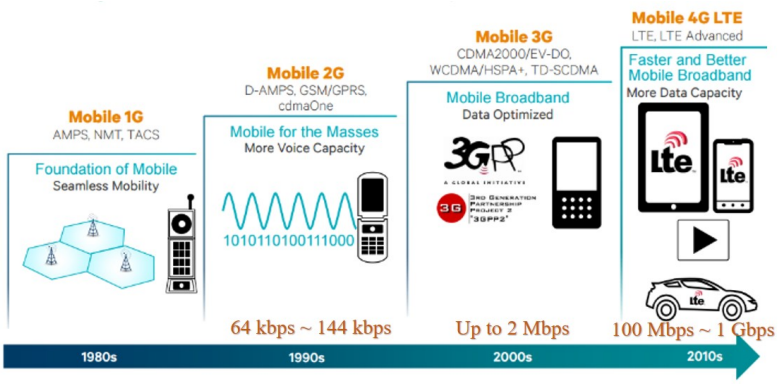

FIGURE 1.1: Evolution of mobile devices [1].

Data rate, bandwidth and also latency of 4G are not quite enough to support more advanced communications like Internet of Things (IoT) such as smart gadgets, wearable devices, smart vehicular communications and etc. [17]. Therefore, since the beginning of 2010, the future generation of wireless communication, 5G, has become a major research area in the telecommunication field. 5G technology aims to provide higher speed between 10 Gbps and 100 Gbps, latency less than 1 ms, 1000 times larger capacity than in 4G, and more than 100 billion connections [17]. Figure 1.2 shows the evolution of mobile devices based on each generation. As it can be seen, in 5G, not only mobile phones and tablets are easily connected, but also each region provided with 5G technology will be easily connected to each other with very high speed and less latency.

FIGURE 1.2: Evolution of mobile devices [2].

1.2 F-OFDM as a waveform Candidate for 5G

OFDM has been widely used as a transmission waveform in 4G/LTE technologies in the recent years. OFDM is designed to provide high spectral efficiency and robustness against multipath fading, which causes ISI [18]. Nowadays, with the advance technologies in wireless communication services, higher data rate and higher spectrum efficiency systems are required, therefore, more researches on next generation of mobile communication, 5G, is in progress. Even though OFDM waveform has many advantages, it is not a suitable waveform candidate for 5G because it suffers from high PAPR and high out-of-band (OOB) emission [19]. High PAPR causes the transmitted signal to get amplified non-linearly, leading to distortion in time domain and OOB spectrum regrowth in frequency domain [11]. High OOB spectrum emission is not desirable since it causes adjacent band interference,hence reduces the spectrum efficiency [11].

According to the 3rd generation partnership project (3GPP) [20][3], 5G is expected to be able to support three significant applications, namely massive machine type communications (mMTC), enhanced mobile broadband (eMBB) and ultra-reliable and low-latency communications (URLLC). The usage of the above future International Mobile Telecommunications (IMT) is illustrated in Figure 1.3. Ideally, 5G waveforms are expected to

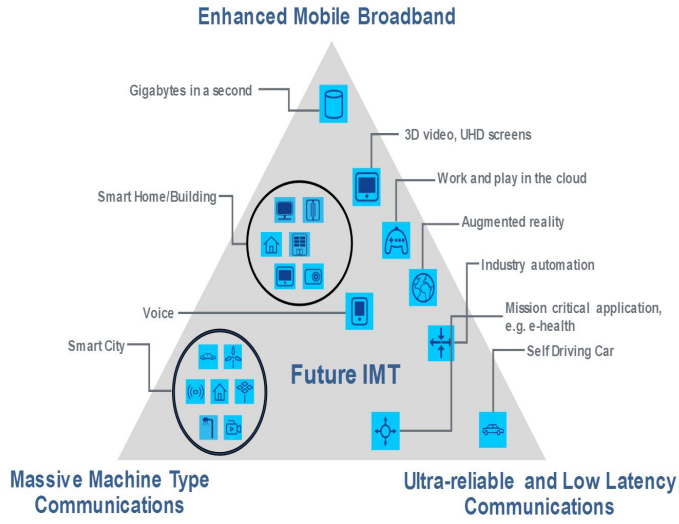

FIGURE 1.3: Usage scenarios of IMT for 2020 and beyond [3]

be able to fulfill the requirements of different types of services and channel characteristics in application like mMTC, generate lower OOB emission and provide asynchronous transmission [4].

Therefore, filtered-OFDM was proposed to satisfy the requirements of 5G systems [21]-[23]. F-OFDM is a modified version of conventional OFDM. F-OFDM splits up the assigned bandwidth of the system into several sub-bands, and each sub-band is processed in OFDM waveform with suitable parameters to accommodate different types of services, and then it is filtered to suppress OOB spectrum, which interferes with its adjacent sub-bands. Thanks to these filters, OOB emission of F-OFDM systems is reduced, thereby spectrum efficiency is improved.

1.3 Motivation

One of the purposes of F-OFDM is to provide much lower OOB emission, which depends on filter designs. To achieve F-OFDM, a digital finite impulse response (FIR) filter is applied on each OFDM symbol after adding cyclic prefix to the symbol. Therefore, proper design of these filters to achieve a very lower OOB emission in F-OFDM becomes crucial. Design of linear-phase FIR digital filter based on window function method has been studied in [24]. FIR filter designed by windowing method is easy and robust, however it does not provide optimum solution. One of the reasons is that windowing does not allow to have different approximation errors (δ) between the required frequency response and the true frequency response in passband and stopband, and the approximation error is less accurate compared to optimal approximation method [7].

On the other hand, optimal approximation methods based on Parks-McClellan algorithm utilize the Chebyshev approximation theory and the Remez exchange algorithm to obtain optimal filters. The filters are optimum when the maximum approximation error is minimized [7]. Parks-McClellan algorithm is used in [25] to design a linear-phase FIR filter for clipping and filtering method of PAPR reducing in OFDM by taking advantage of out-of-band radiation reducing property of the filter. Therefore, in this study, Parks-McClellan algorithm is proposed in designing the filter instead of window function and other common methods.

We observe that the effect of high power amplifier (HPA) on F-OFDM has not been studied in a greater detail. Passing the F-OFDM signals through a HPA at the transmitter end causes OOB spectral regrowth due to non-linear behavior of power amplifier. Hence, there is a need to compensate for the non-linearity effects in baseband domain

since techniques of reducing spectral regrowth in passband requires higher complexity and cost [11]. Applying digital baseband pre-distortion (DPD) before the high power amplifier allows low OOB emission with relatively less complexity and cost [26][27]. Since F-OFDM signal is a wideband signal, memory effect of power amplifier must be taken into consideration in designing pre-distorter.

Even though F-OFDM with Parks-McClellan filter has a much lower OOB emission and the same bit error rate (BER) compared to OFDM, PAPR of F-OFDM signals becomes higher. This is due to the longer filter tails caused at head and tail of the time domain F-OFDM signal [4].PAPR is defined as the ratio between maximum power and average power of the transmitting symbol. Hence, with the same peak power as OFDM signals, smaller values of the f-OFDM tails cause smaller average power, resulting in higher PAPR. Hence, we will also perform the PAPR reducing procedure on the F-OFDM signal and analyze the results.

One way to reduce PAPR is through iterative clipping and filtering (ICF) approach. ICF is a simple technique to reduce PAPR to a desired threshold, however, due to amplitude distortion and out-of-band spectral regrowth caused by clipping in time domain and peak regrowth caused by filtering with a ideal filter in frequency domain, conventional ICF requires several iterations to reach to the desired threshold. Hence, optimization is required to satisfy both PAPR and OOB emission requirement. Many studies have used convex optimization for reducing PAPR of OFDM signals due to the fact that it can guarantee a global optimal solution with efficient computation [28]. Therefore, convex optimization technique is applied to the conventional ICF method to obtain a desired PAPR reduction while maintaining a low OOB emission with fewer iterations [28]. In this study, we modified the optimized ICF used in [28] to be suitable for F-OFDM signals.

Many studies focus mainly on the basis F-OFDM system with BER and OOB emission performance [4]-[24][19], yet neglect the other aspects of the system, such as PAPR. Therefore, in this paper, PAPR and OOB reduction techniques, such as optimized ICF and pre-distortion, are also included in the system. Simulation results show that in the presence of non-linear power amplifier, F-OFDM system composed of the proposed optimized ICF and DPD achieves better BER performance with smaller PAPR and lower OOB emission compared to the optimized signal without DPD.

1.4 Conclusion

In this chapter, F-OFDM technology was briefly introduced. Moreover, the motivations behind performing the F-OFDM system with PAPR reducing technique and predistortion have been explained. In order to observe the performance of OOB emission, PAPR and BER performance of F-OFDM signal clearly, in this thesis, we will conduct the performance analysis on each part of the system mentioned above and overall system. Before discussing the performance of the F-OFDM system, literature reviews on the work related to F-OFDM will be firstly presented in Chapter 2. Then, Chapter 3 will discuss the analysis of the basis F-OFDM system with different filtering methods, and Chapter 4 will show the effect of PA and simulation of the updated system with DPD. In Chapter 5, optimized ICF, which is a PAPR reducing technique, will be discussed, and simulation of the full system will be analyzed. Finally, the thesis will be concluded with the final chapter, stating the summary and the future works.

Chapter 2

Literature Review

Throughout this chapter, the literature background of the previous state of the art related to F-OFDM will be given. Moreover, at the end of the chapter, the contributions of this thesis will be re-iterated.

2.1 Literature Background

In 5G, much higher bandwidths between 100 MHz to 200MHz are expected to be utilized. For such large bandwidths, F-OFDM is a good waveform candidate, which utilizes the available bandwidth efficiently by dividing it into many sub-band and employing OFDM with different waveform parameters according to the needs of the services to be provided. Unlike OFDM, F-OFDM has the time and frequency flexibility to support different types of services within the same bandwidth given [4]. Figure 2.1 shows the time and frequency flexibility in F-OFDM system for a given bandwidth. As an example, in the case of IoT technology, a single-carrier modulation system with a long transmission time interval (TTI) may be employed instead of an conventional OFDM system. On the other hand, in vehicle to vehicle (V2V) communication environment, which requires much lesser latency, a basic OFDM scheme with very large sub-carrier spacing may be used, so that much shorter TTI can be provided. Therefore, with the F-OFDM system, different types of modulation with different numerology can be integrated based on the requirements of the services and available wireless channel types [4].

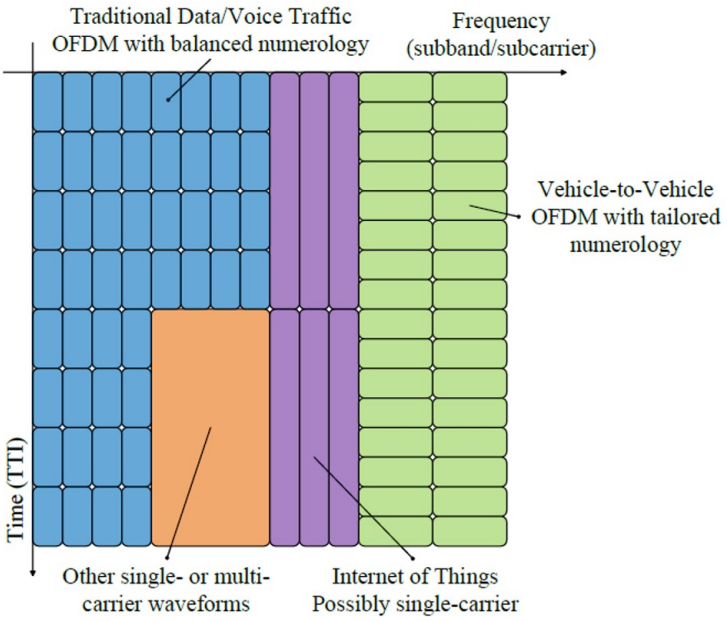

FIGURE 2.1: Flexibility of F-OFDM system [4].

F-OFDM is a modified system of OFDM by means of sub-band filtering. Filtering has been generally used in OFDM system to improve spectrum localization [29][30]. Apart from F-OFDM, universal-filtered OFDM (UF-OFDM) or universal-filtered multicarrier (UFMC), which are also based on sub-band filtering of OFDM signals, was introduced in [22][31]. The comparison of the conventional pulse-shaped OFDM, F-OFDM, and UF-OFDM can be presented as follows:

1. In the conventional pulse-shaped OFDM, sub-carrier based pulse shaping is done by applying filter on each CP-OFDM symbol. On the other hand, in F-OFDM, sub-band based filtering is performed on each OFDM signal which consists of more than one CP-OFDM symbol within a sub-band to mitigate the OOB emission.

2. While UF-OFDM system performs sub-band filtering zero prefix (ZP) OFDM signal, in F-OFDM system, it is done on CP-OFDM signal. Since F-OFDM is based on CP-OFDM, the issue with ISI can be mitigated and hence channel equalization becomes less complex compared to UF-OFDM system. Moreover, in UF-OFDM, the filter length cannot exceed ZP length, in order to avoid ISI. On the other hand, F-OFDM allows the filter length longer than the length of the CP, to be able to support better time and frequency localization.

The advantage F-OFDM over OFDM can also be summarized as follows: [24][4]:

1. Due to the sub-band based filtering, reduced OOB emission can be achieved. Therefore, lesser guard band can be applied unlike OFDM, which uses 10% of its given bandwidth in 4G as a guard band at both end of the bandwidth. Hence, F-OFDM scheme can provide better spectrum efficiency than OFDM scheme.

2. In addition, the reduced OOB emission provided by the sub-band based filtering in F-OFDM, asynchronous transmission across sub-bands can also be employed. This is due to the fact that sub-band filtering purposely breaks the time-domain orthogonality between different user equipments (UEs), so that time advance signaling for synchronization can be neglected. On the other hand, in OFDM, heavy synchronization signal is required to maintain the orthogonality. Figure 2.2 shows the asynchronous transmission supported by a F-OFDM system.

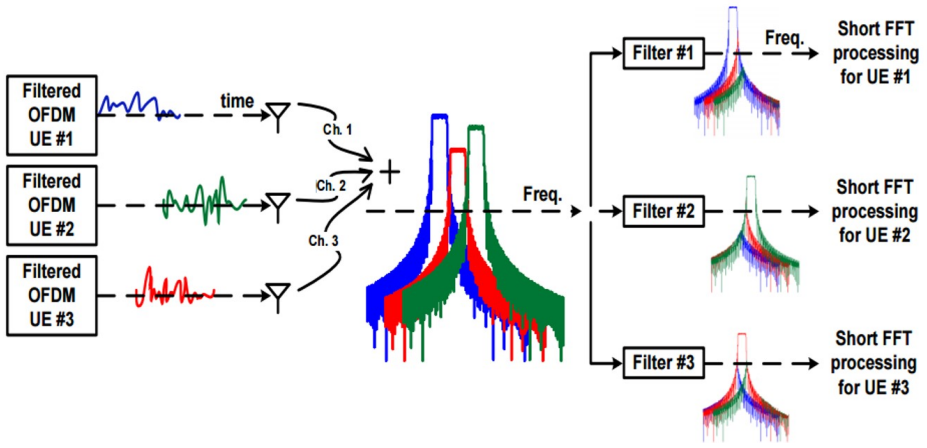

FIGURE 2.2: Asynchronous transmission of a F-OFDM system [5].

3. The most important advantage of F-OFDM system is that its ability to provide unified numerology with different time and frequency requirements according to the types of applications within the available bandwidth. The coexistence of different modulation scheme and flexibility of F-OFDM has already been explained in Figure 2.1. In contrast, OFDM cannot provide different parameters required by the different types of transmission at the same time.

Many studies have been done relating to F-OFDM. According the study in [4], the authors are convinced that F-OFDM can be adopted in 5G from 4G easily. Figure 2.3 describes the possible evolution of F-OFDM in 5G from OFDM in 4G. 4G technology uses 10% of the assigned bandwidth as a guard band. At the beginning of the development, this guard band will also be used for transmitting data via F-OFDM, so that the current

communication technologies built with 4G can still be used. In the future, the assigned bandwidth of 4G will become smaller, and 5G will utilize the rest of the bandwidth through F-OFDM scheme, in order to provide better spectrum efficiency.

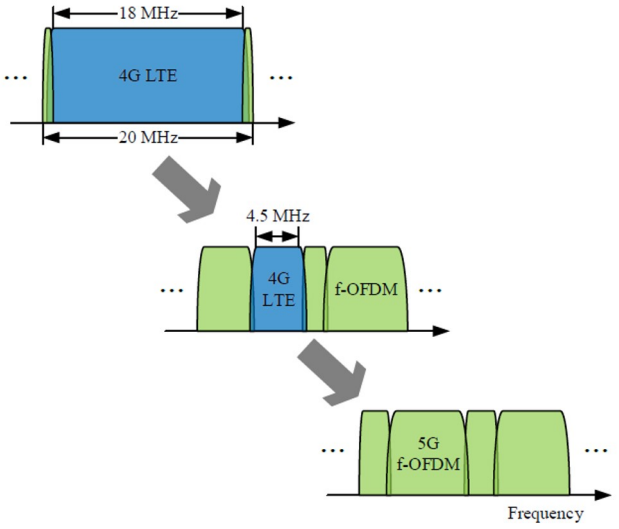

FIGURE 2.3: Evolution of OFDM to F-OFDM [4].

Performance comparison of F-OFDM system within different scenarios are mostly studied in the literature. In [4], the performance of F-OFDM scheme of the first stage and the last stage of the evolution diagram shown in Figure 2.3 was performed. For the first part, both guard bands and the main band of 4G are considered as sub-bands, and conventional OFDM with the same parameters are applied in each sub-band. Performance evaluation was done by analyzing block error rate (BLER) and PSD. As for the final stage, the authors tested the flexibility of F-OFDM system by using 4 types of communication scenarios; pedestrian, urban, highway, and V2V; assigning each to a sub-band and comparing their throughput with OFDM. From their findings, the authors concluded that F-OFDM systems can support different channel requirements in addition to smaller guard bands. The detailed throughput comparison of the F-OFDM system with OFDM system is illustrated in Figure 2.4.

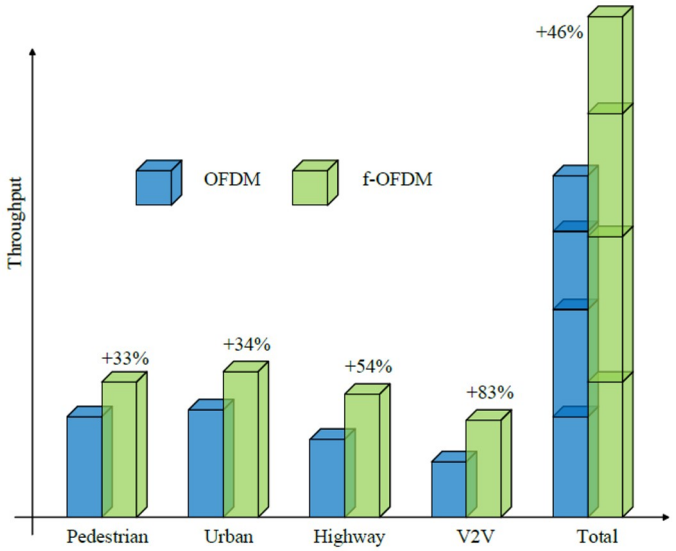

FIGURE 2.4: Throughput comparison of F-OFDM system with OFDM system [4].

Filtering is the key process in F-OFDM system, and therefore a good filter design is very important. Not many studies discuss the detailed analysis of the effect of different filtering methods on F-OFDM signals. In [24], the authors proposed a simple filtering method based on window function. A FIR digital filter was designed by soft truncating the ideal rectangular filter in frequency domain with different window type. Their simulation results showed that window based filters can be implemented easily and it also gives a large reduced OOB emission while maintaining the same BER performance of OFDM signal. In this thesis, the detailed comparison of this method and Parks-McClellan method will be analyzed in the next chapter.

As mentioned above, for the advantages of F-OFDM scheme, inter-sub-band asynchronous transmission can be provided by a F-OFDM system. In [6], this property of F-OFDM was verified. Moreover, the authors also introduced F-OFDM based multiple access (MA) technique known as an asynchronous F-OFDMA or filtered discrete-Fourier transform-spread OFDMA (f-DFT-S-OFDMA) scheme. The system diagram of f-DFT-S-OFDMA scheme proposed in [6] is shown in Figure 2.5.

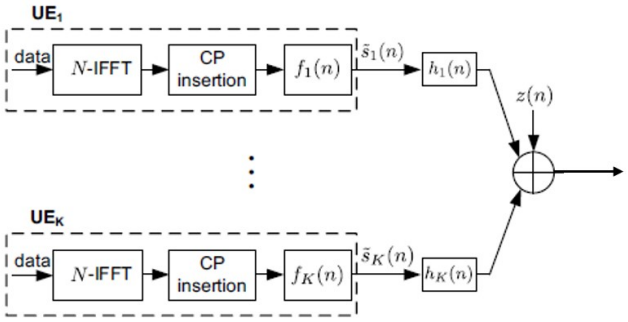

(A) Transmitter

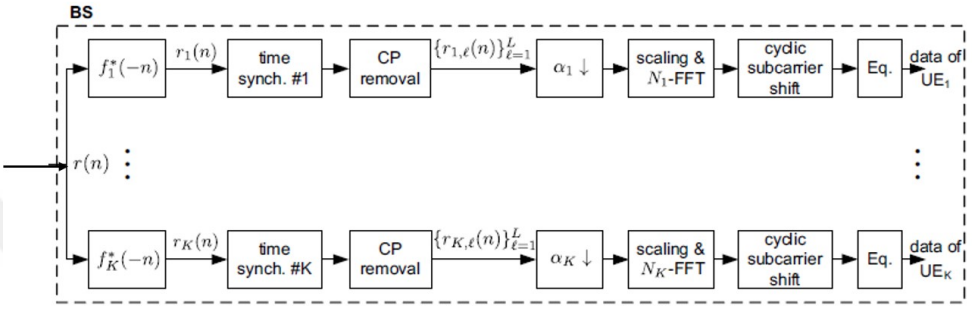

(B) Receiver

FIGURE 2.5: Asynchronous F-OFDMA/f-DFT-S-OFDMA [6].

At the transmitter side, each sub-band is allocated to each UE and DFT-S-OFDM signal resulting from each UE is filtered with a filter to reject the OOB spectrum leakage. All the f-DFT-S-OFDM signals are combined and transmitted to a base station (BS). At the BS, matched filtering is performed on the received signal by letting the signal from the UE which uses the same filter at the transmitter side while rejecting the signals from the other UEs. Then, time synchronization is performed on each filtered signal by shifting it by the amount of the respective filter length. The authors observed that compared to the conventional synchronous OFDMA/DFT-S-OFDMA, this proposed scheme does not require the time-synchronization overhead used to avoid inter-sub-band interference at the receiver. From this study, it is also worth noticing that the filter with respect to each UE is designed according to its sub-band bandwidth, hence the filter parameters are available in both BS and UE. Therefore, no signaling overhead caused by employing the filters is occurred.

Apart from the simulation based studies mentioned above, the studies in [32] and [33] continues the analysis of F-OFDM system by performing field trials. The author in [32] carry out the F-OFDM field trial in 5G environment and verify that F-OFDM can provide lesser OOB emission and support asynchronous transmissions. The study in [33]

conducts the OFDM based waveforms field trails with mixed numerologies, and compares the performance of the conventional CP-OFDM, Windowing-OFDM (W-OFDM) and F-OFDM. It is concluded that F-OFDM performs better than both CP-OFDM and W-OFDM in respect of spectral efficiency and robustness in high SNR. In both studies, root-raised cosine (RRC) window based filtering method is applied.

2.2 Thesis Contributions

In the literature, there are several studies on the F-OFDM scheme for 5G technology. Many of them concentrate solely on F-OFDM's performance regarding OOB spectrum leakage and BER without considering the effect of high PA in the system. In practical communication system, HPA is not always linear, hence high PAPR signal such as OFDM and F-OFDM signals normally suffer from the non-linear behaviour of the PA, however implementing a linear PA is costly and not power efficient [34].

Therefore, there is a need to analyze the effect of non-linear PA in a given F-OFDM system, a strong candidate of the future wireless communication technology. Throughout this study, BER performance will be assessed in an AWGN channel to focus on the system alone. The evaluation of F-OFDM will be done in three stages:

Firstly, simulations will be performed comparing out-of-band emission and BER of F-OFDM signals obtained from different filtering techniques.

Secondly, conventional PA will be applied in the system and its effect will analyzed. Then, linearization technique based on pre-distortion will be also added before the PA, and the performance will be discussed in terms of OOB power spectrum emission and BER.

Lastly, optimized ICF will be used to reduce the PAPR of F-OFDM, then the resulting optimized F-OFDM signal will go through the pre-distortion process. At the end, simulation of this overall system will be performed.

By integrating the optimized ICF and DPD into the basis F-OFDM system, a good performing system in the presence of conventional PA is achieved.

Chapter 3

Performance Analysis of F-OFDM using Parks-McClellan Filter

In this chapter, basis structures of OFDM and F-OFDM transceivers will be firstly described. Then, the design of filter based on windowing method and Parks-McClellan algorithm will be discussed. Lastly, the performance F-OFDM with Parks-McClellan filter will be compared with the window based filters.

3.1 F-OFDM Basis

In recent years, OFDM has been a popular multi-carrier modulation technique used in wide-band digital communication such as 4G/LTE. However, with the advances in application available in 5G system, OFDM waveform does not have the ability to provide the requirements of 5G. Therefore, researchers has been developing new waveforms suitable for 5G systems, and F-OFDM is one the promising candidates.

3.1.1 Conventional OFDM Transceiver

In OFDM transmitters [24], as depicted in Figure 3.1, a sequence of binary data bits are firstly generated and mapped to complex data symbols (sub-carriers) by using M order quadrature amplitude modulation (M-QAM) technique, which is used in LTE system. Then, the serial sub-carriers are converted into parallel sub-carriers, and a group

consisting N_{sub} numbers of sub-carriers produces one OFDM symbol. Each sub-carriers group is oversampled with a factor of L by $(L-1)N_{sub}$ zeros padding, and a OFDM symbol is obtained by applying N-point IFFT , where $N = LN_{sub}$ is the IFFT/FFT size. Therefore, each OFDM symbol has N_{sub} numbers of sub-carriers in frequency domain.

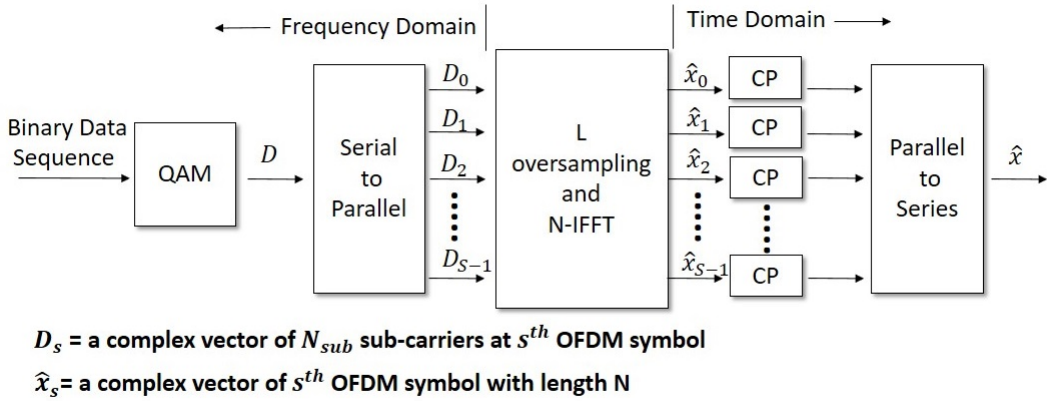

FIGURE 3.1: Transmitter Structure of OFDM System.

Mathematically, a discrete time OFDM symbol, $\hat{x}_s(n)$, can be presented as [28] :

$$\hat{x}_s(n) = \frac{1}{\sqrt{N}} \sum_{i=1}^{N_{sub}} D_s(i) e^{j\frac{2\pi n}{N} i} \tag{3.1}$$

where n denotes discrete-time index as $n = 1, \ldots, N$ and i is sub-carriers index as $i = 1, \ldots, N_{sub}$. D_s represents a complex vector of sub-carriers at s^{th} symbol. After generating the OFDM symbol, CP with length N_{cp} is then inserted in each OFDM symbol, and summation of S numbers of them results in a single OFDM signal, $\hat{x}(k)$, at the transmitter as:

$$\hat{x}(k) = \sum_{s=0}^{S-1} \hat{x}_s(k - s(N + N_{cp})), \quad -N_{cp} < k < N \tag{3.2}$$

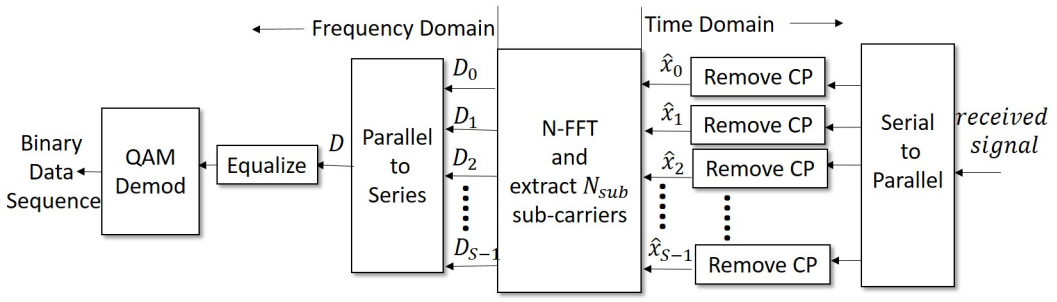

FIGURE 3.2: Receiver Structure of OFDM System

OFDM receiver operates as a reverse process of the transmitter as illustrated in Figure 3.2. At the receiver, after removing the CP of each OFDM symbol, each received symbol, $\hat{r}_s(n)$, is converted into frequency domain symbols by applying N-point FFT, which can be represented as [28]:

$$D_s(i) = \sqrt{N} \sum_{n=1}^{N} \hat{r}_s(n) e^{-j\frac{2\pi n}{N} i} \tag{3.3}$$

Then, frequency domain channel estimation and equalization is performed, and the resulting symbols are demodulated into the data bits.

3.1.2 F-OFDM Transceiver

Basically, a F-OFDM signal is obtained from multiple OFDM signals by suitable filtering method. Both transmitter and receiver structures are described in Figure 3.3 and Figure 3.4, respectively. As shown in F-OFDM transmitter, Figure 3.3, a given available bandwidth is divided into multiple sub-bands, and each sub-band undergoes through the OFDM scheme with the same or different parameters; N_{sub}, N, N_{cp} and S; accordingly. A F-OFDM signal at g^{th} sub-band, $x_g(k)$ is obtained by filtering the resulting CP-OFDM signal, $\hat{x}(k)$, with a suitable filter, $f(k)$, and it can be expressed as a linear convolution process in time domain as [24]:

$$x_g(k) = \hat{x}(k) * f(k) \tag{3.4}$$

Due to the fact that the addition of CP in OFDM signal transforms the linear convolution into circular convolution, the convolution process in time domain can take alternative

form in frequency domain as the element-wise multiplication [7]. Therefore, filtering process in frequency domain can be written as simple multiplication of the Fourier transform of $\hat{x}(k)$ and $f(k)$:

$$X_g(e^{j2\pi f}) = \hat{X}(e^{j2\pi f}) \cdot F(e^{j2\pi f}) \tag{3.5}$$

where "$\cdot$" represents element-wise multiplication.

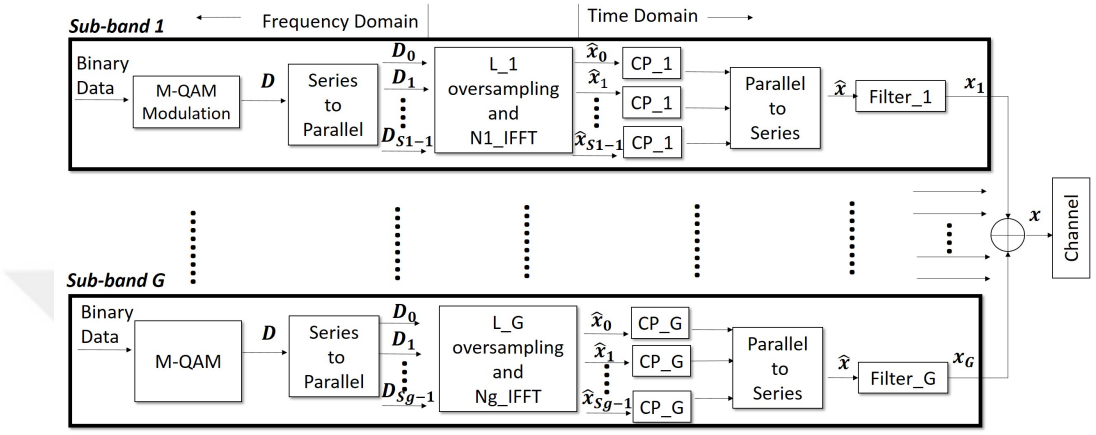

FIGURE 3.3: Transmitter Structure of F-OFDM System

All F-OFDM signals at different sub-bands are then concatenated and transmitted through a wireless channel. At the receiver, a matched filter of respective transmitter filter, $f^*(-k)$, is applied on the received signal so that signal at desired sub-band can be retrieved. The received filtered signal at g^{th} sub-band, $r_g(k)$, can be written as [6]:

$$r_g(k) = \Big(\Big(x_g(k) * c(k)\Big) + w(k)\Big) * f^*(-k) \tag{3.6}$$

where $c(k)$ and $w(k)$ are wireless channel impulse response and AWGN noise, respectively.

Then, the filtered signal is split into OFDM symbols followed by CP removal block and N-FFT block. Next, channel estimation and equalization is performed on the resulting signal to compensate the effect of both filters and the channel. Lastly, the data symbols are selected from the equalized sub-carriers and then demodulated into a binary stream [6]. The receiver structure of the F-OFDM system is illustrated in Figure 3.4.

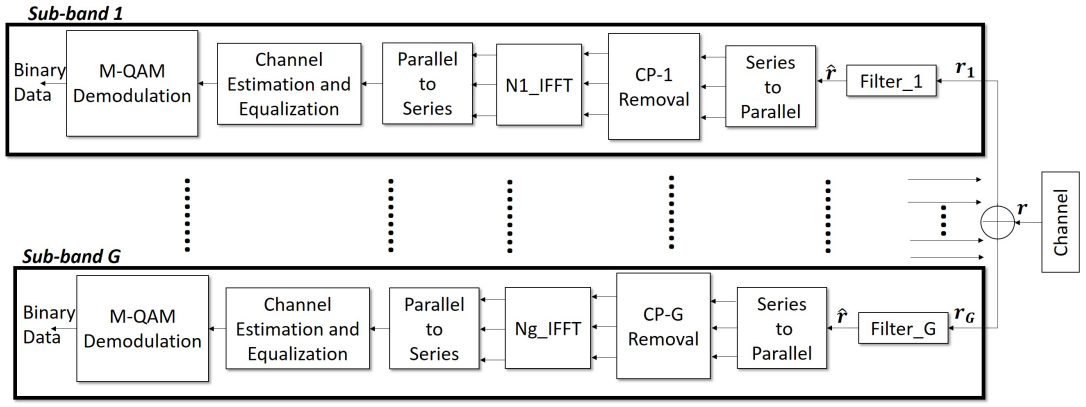

FIGURE 3.4: Receiver Structure of F-OFDM System.

3.2 Filter Design

The major process in F-OFDM system is the design of filters used since they affect the OOB emission performance of the signal. In [24], the authors discuss about the criteria for designing the digital FIR filter for F-OFDM signals. It is stated that a very narrow filter transition band (Δf), which is between passband and stop- band, is preferable since it allows lesser OOB emission. Moreover, the filter should not have attenuation in the main band not to have any loss of the signal passing through the filter, and it should use lower stopband attenuation as well. Therefore, an optimum algorithm is used to design filters with different desired passband and stopband ripple attenuation and narrower transition band. In this thesis, firstly, we will present a brief discussion about window-based FIR filter design and then explain the Parks-McClellan optimum algorithm.

3.2.1 Window-based FIR Filter

Many studies have been performed for F-OFDM system analysis with window-based FIR filter [4, 6, 24]. In windowing method, as shown in Figure 3.5, the width of transition band of resulting filter depends on the width of main lobe, Δf_m, of the Fourier Transform of the window, and stopband and passband ripples depends on the side lobes of the Fourier Transform of the window. Thus, the width of main lobe and peak side lobe magnitude δ of the window must be small in order to obtain small transition band and less ripples.

Here $W(e^{j2\pi f})$, $F(e^{j2\pi f})$, and $F_d(e^{j2\pi f})$ are Fourier Transform of the windowing function, desired response and the resulting windowed response respectively. [7].

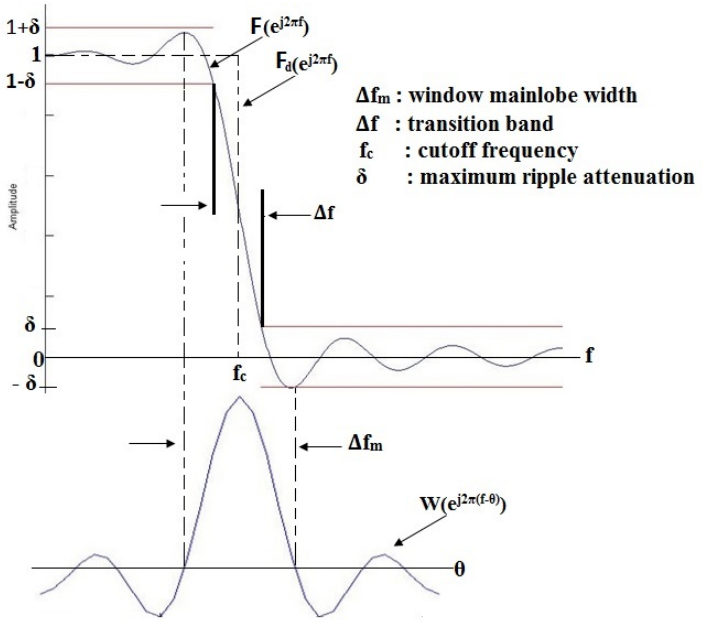

FIGURE 3.5: Windowing method in frequency domain [7].

The frequency response of the ideal low pass filter is a rectangular function as shown in Figure 3.5 [7], and the impulse response is a *sinc* function, which has infinite delay and thus difficult to implement as a real-time filter. Hence, the *sinc* function is soft-truncated with a suitable window function by multiplying in time domain as [7][24]:

$$f(k) = w(k).f_d(k) \tag{3.7}$$

where $w(k)$ and $f_d(k)$ impulse response of the window function and the desired filter. Figure 3.6 demonstrate the soft-truncation of impulse response of the ideal low pass filter in time domain.

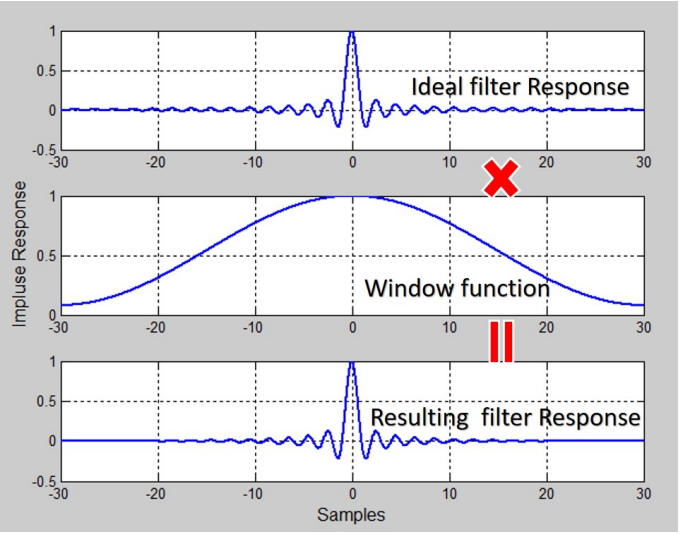

FIGURE 3.6: Example of soft-truncating a ideal filter.

Different window functions provide different passband and stopband attenuation and coefficients to the resulting filter, which lead to different OOB leakages of F-OFDM signals. Some of the window functions discussed in literature are [29]:

- Kaiser:

$$w(k) = \frac{I_0\left(\beta\sqrt{1-\frac{4k^2}{(N_w-1)^2}}\right)}{I_0(\beta)}, \quad \frac{-(N_w-1)}{2} \leq k \leq \frac{(N_w-1)}{2} \tag{3.8}$$

  where I_0 is the modified zero-th order Bessel function of the first kind, and β is the attenuation parameter given as:

$$\beta = \begin{cases} 0.1102(\alpha - 8.7), & \alpha > 50 \\ 0.5842(\alpha-21)^0.4 + 0.07886(\alpha-21), & 21 \leq \alpha \leq 21 \\ 0, & \alpha < 21 \end{cases} \tag{3.9}$$

  where α is side-lobe attenuation. Figure 3.7 describes the effect of β values on main-lode width and side-lode amplitude. As β increases, amplitude of the side-lobes reduces and the main-lobe width become wider.

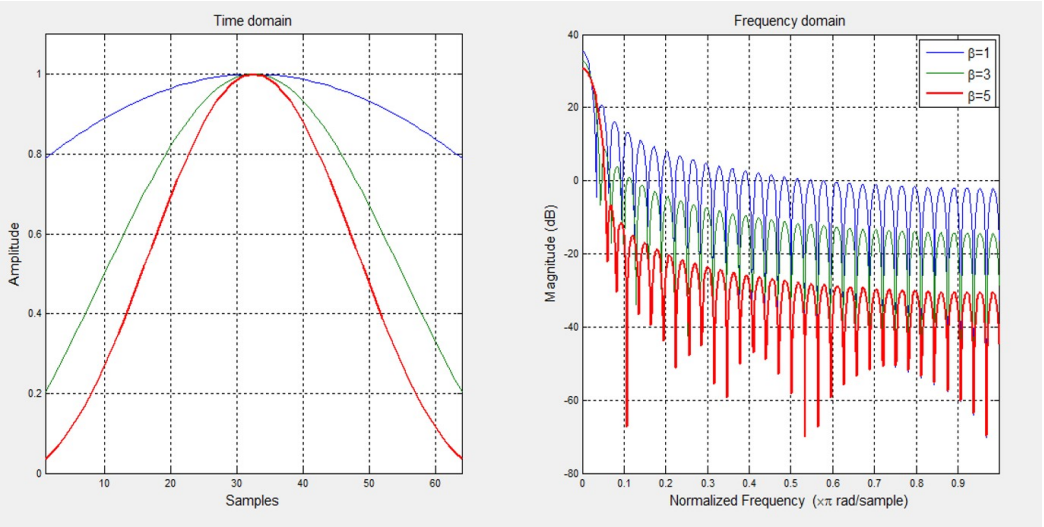

FIGURE 3.7: Time and frequency domain responses of Kaiser window with length=64

- Gaussian [35]:

$$w(k) = e^{\frac{-1}{2}(\alpha \frac{k}{(N_w-1)/2})}, \quad \frac{-(N_w-1)}{2} \leq k \leq \frac{(N_w-1)}{2} \tag{3.10}$$

where $\alpha = \frac{(N_w-1)}{2\sigma}$, and σ is the standard deviation a Gaussian random variable. As illustrated in Figure 3.8, increasing the value of α results in a narrower window in time domain.

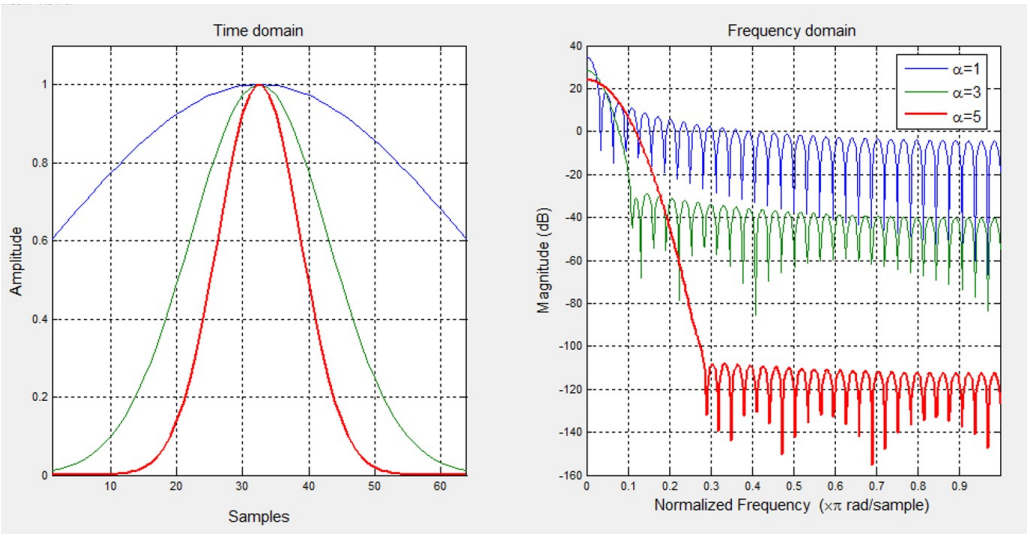

FIGURE 3.8: Time and frequency domain responses of Gaussian window with length=64

- Hamming:

$$w(k) = 0.54 - 0.46\cos(\frac{2\pi k}{N_w}), \quad 0 \leq k \leq N_w \tag{3.11}$$

- Chebyshev:

$$w(k) = \frac{1}{N_w}\left[\frac{1}{r} + 2\sum_{i=1}^{(N_w-1)/2} T_{N_w-1}\Big(x_0 \cos(\frac{i\pi k}{N_w})\Big) \cos(\frac{2\pi ki}{N_w})\right], \quad 0 \le k \le N_w [36] \tag{3.12}$$

where r is the desired passband ripple, and x_0 is defined as

$$x_0 = \cosh(\frac{1}{N_w - 1}\cosh^{-1}(\frac{1}{r})) \tag{3.13}$$

$T_n(x)$ in the equation 3.12, which is chebyshev polynomial of the first kind, is formulated as

$$T_n(x) = \begin{cases} \cos(k\cos^{-1}(x)), & |x| \le 1 \\ \cosh(k\cosh^{-1}(x)), & |x| > 1 \end{cases} \tag{3.14}$$

- Hann:

$$w(k) = 0.5 - 0.5\cos(\frac{2\pi k}{N_w}), \quad 0 \le k \le N_w \tag{3.15}$$

- Blackman:

$$w(k) = 0.42 - 0.5\cos(\frac{2\pi k}{N_w - 1}) + 0.08\cos(\frac{4\pi k}{N_w - 1}), \quad 0 \le k \le N_w - 1 \tag{3.16}$$

- Blackman-Harris:

$$w(k) = 0.35875 - 0.48829\cos(\frac{2\pi k}{N_w - 1}) + 0.14128\cos(\frac{4\pi k}{N_w - 1}) - 0.01168\cos(\frac{6\pi k}{N_w - 1}), \quad 0 \le k \le N_w - 1 \tag{3.17}$$

where $N_w + 1$ gives the window length. Figure 3.9 shows the time and frequency domain response of the window functions listed above.

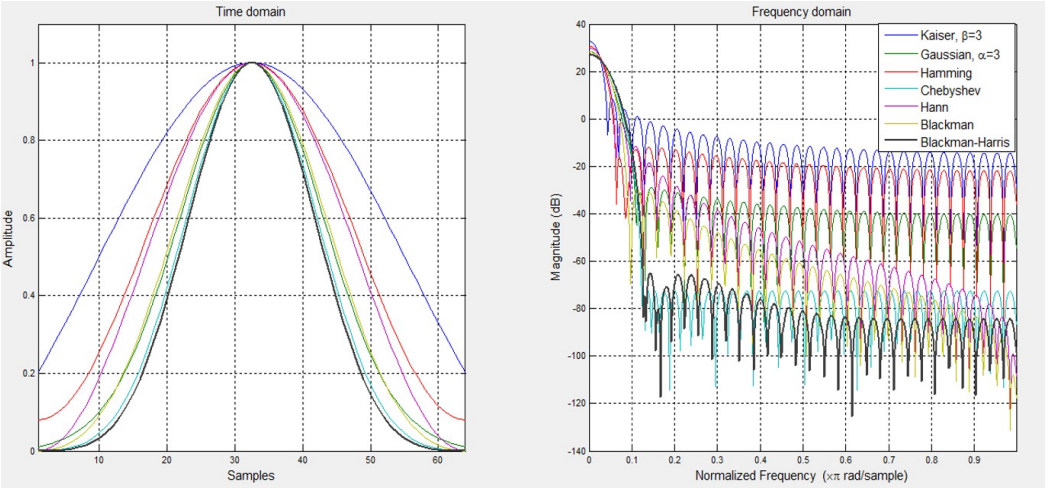

FIGURE 3.9: Time and frequency domain responses of window functions with length=64

After truncating the ideal filter with the different window functions, power spectrum density of the filters are shown in Figure 3.10. The same filter order is used for all the filters for a fair comparison. As shown in the PSD diagram, Kaiser filter generates a highest stopband attenuation, resulting in higher OOB emission. On the other hand, Blackman-Harris filter has a lowest stopband attenuation and hence, it is a favorable window for lower OOB emission. Among the window functions, Chebyshev filter has the narrowest transition band, yet higher stopband attenuation. Therefore, there is no perfect window based filter which fulfills all the criteria needed for designing filter of F-OFDM system. Hence, window-based filters cannot provide the appropriate filtering for F-OFDM system since the filter should have narrow transition band, low stopband attenuation, and flat passband. However, none of the window-based filters have all these properties in just one filter.

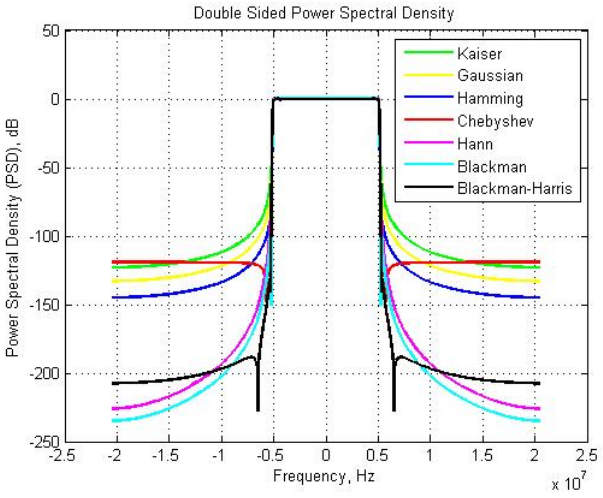

FIGURE 3.10: PSDs of window based filters

FIR filter design by windowing method is powerful and simple, but it is not a optimum filter due to the following reasons [7]:

1. Windowing does not allow to have different maximum approximation errors, δ, in passband and stopband ($\delta = \delta_p = \delta_s$). This is not preferable when specification is stricter in the stopband than in the passband.

2. The ripples of the window are not uniform, but they die out slowly as it moves away from discontinuity points according to side-lobe structure of the window, which results in higher filter's order.

3. Approximation error δ is less accurate compared to optimal approximation method.

3.2.2 Parks-McClellan FIR Filter

Parks-McClellan FIR filter applies Chebyshev approximation theory and Remez exchange algorithm to design optimum filters. The filters are considered to be optimum when the maximum error between the resulting frequency response and the desired frequency response is minimum [7, 9]. The resulting filters minimize the maximum error by distributing the weighted approximation error evenly across respective band. This kind of filters which show equiripple behavior (ripples fluctuate uniformly between the maximum and minimum ripple amplitudes) in both the stopband and the passband are also known as equiripple filters. The procedure of Parks-McClellan algorithm based on Remez exchange algorithm is described in Figure 3.11, and the steps are explained as follow [7][8][9]:

1. Initialize L+2 extremal frequencies (w_k) between 0 and π as a reference frequency set, where L is order of the filter and $k = 0, \ldots, L+1$.

2. Compute δ using the equation 3.18

$$\delta = \frac{\sum_{k=0}^{L+1} \gamma_k A_d(w_k)}{\sum_{k=0}^{L+1} \frac{(-1)^k \gamma_k}{W(w_k)}} \tag{3.18}$$

   where $A_d(w_k)$ is a sample of desired amplitude response $A_d(w)$, and $W(w_k)$ is a sample of weight function $W(w)$. γ_k is calculated as:

$$\gamma_k = \prod_{\substack{i=0 \\ i \neq k}}^{L+1} \frac{1}{cos(w_k) - cos(w_i)} \tag{3.19}$$

3. Given extremal frequencies and the calculated δ, compute L+2 samples of $A(w_k)$ by using Lagrange Interpolation, which can be directly obtained as:

$$A(w_k) = A_d(w_k) - \frac{(-1)^k}{W(w_k)}\delta \tag{3.20}$$

4. Obtain the weighted approximation error function, $E(w) = W(w)(A_d(w) - A(w))$, over the current extremal frequencies.

5. If $|E(w_k)| \leq \delta$, the optimum δ is achieved. Otherwise, locate the new L+2 frequency set at the local extrema errors where $|E(w_k)| > \delta$ for each w_k.

6. This process starting from the step (2) is iterated until δ obtained from the new extremal frequencies does not change any more.

7. After obtaining the optimum δ, compute the time domain filter response, $h(n)$, by inverse Fourier transform of $A(w)$.

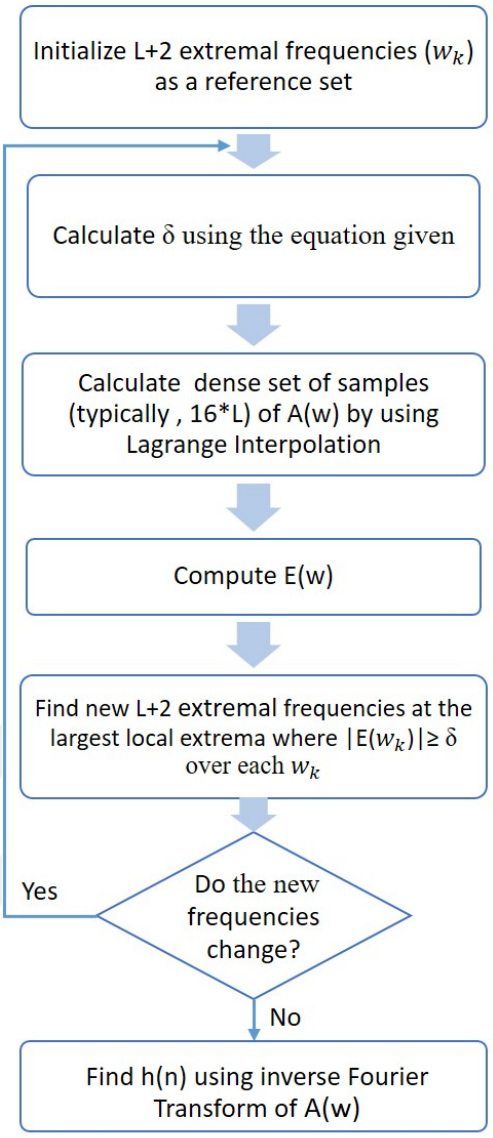

FIGURE 3.11: Flowchart of Parks-McClellan algorithm [7][8][9]

In this study, Parks-McClellan FIR filter is implemented via MATLAB build in function called $firpm()$. Figure 3.12 exhibits the frequency response of Parks-McClellan filter with different values of δ_s. It can be seen that lower OOB emission can be obtained by choosing smaller value of δ_s, but it results in higher filter's order.

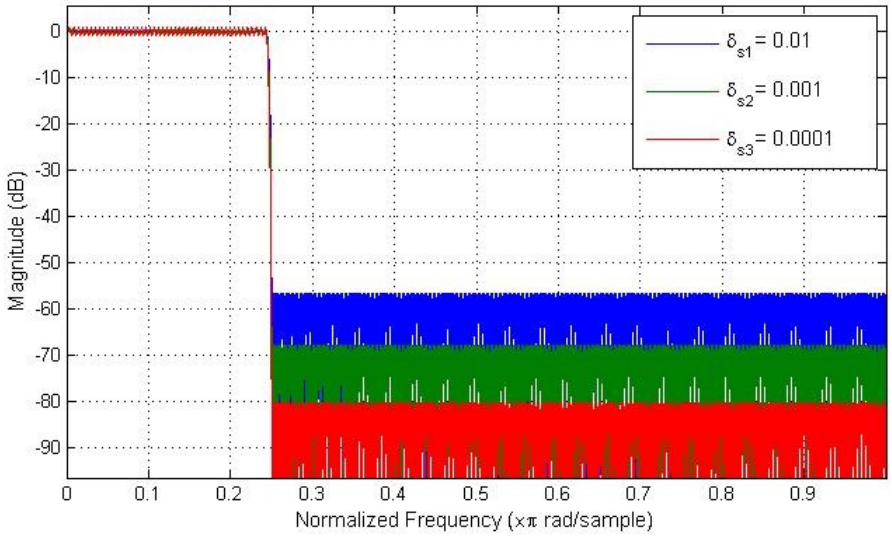

FIGURE 3.12: Frequency response of Parks-McClellan filter with different δ_s values

Figure 3.13 compares the PSD of Parks-McClellan filter with the filters based on Kaiser window, Hamming window, Chebyshev window and Blackman-Harris window. They all have the same order of 1500, which is a minimum order of Parks-McClellan filter for the desired cut-off frequency of 5.06 MHz with $\delta_s = 10^{-8}$ and $\delta_p = 10^{-1}$.

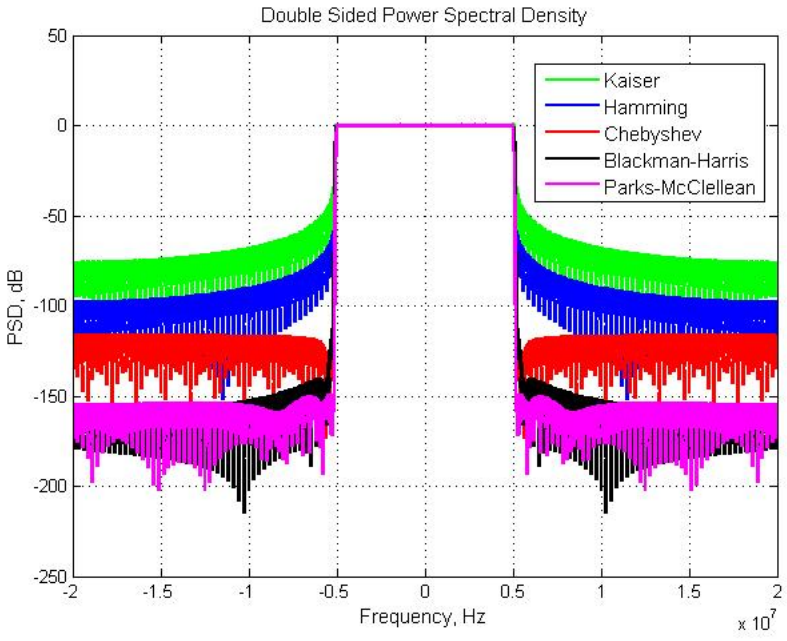

FIGURE 3.13: PSDs of Parks-McClellan filter with $\delta_s = 10^{-8}$ and window based filters

From the analysis of the Figure 3.12 and Figure 3.13, the advantages of Parks-McClellan filter for f-OFDM systems can be summarized as follows:

1. The filter has equal ripples in both passband and stopband respectively, hence in-band spectrum of the f-OFDM signal can be obtained evenly and OOB spectrum can also be suppressed uniformly.

2. Since the filters can set different maximum passband and stopband ripple errors($\delta_p \neq \delta_s$), the in-band and the out-band spectrum of the f-OFDM signals can be adjusted differently according to the requirements of the 5G systems.

3. By selecting the smaller value of δ_s, f-OFDM signal which has lower OOB emissions can be achieved.

4. The transition bandwidth of the f-OFDM signal obtained from Parks-McClellan filter is much narrower than the other methods. It is preferable for the filter design since spectrum leakage can be avoided.

3.3 Simulation and Analysis

In this section, performance of F-OFDM for one sub-band is discussed. All the simulations in this study are done in MATLAB. The simulation parameters of a point-to-point downlink (from a BS to a UE) are given in Table 3.1. The filter used at the transmitter is Type I linear-phase FIR filter, which has even filter order, and the sampling frequency to generate the filter impulse response is calculated from the equation given below (3.21).

$$f_s = \frac{B}{N_{sub}} N \tag{3.21}$$

In this simulation, wireless channel is AWGN and the same filter is applied at the receiver. Channel estimation is performed by pilot interpolation and the received signal is equalized by zero-forcing equalizer to compensate for the effects of the wireless channel and both filters.

Here, we are evaluating the F-OFDM signal which corresponds to a sub-band with the bandwidth of 10 MHz. The filter order of all the filters are based on the minimum order needed for Parks-McClellan filter with passband frequency, $f_{ps} = 5$ MHz, stopband frequency, $f_{st} = 5.12$ MHz.

Table 3.1: Simulation Setup

Parameter	**Value**
sub-band bandwidth (B)	10 MHz
IFFT/FFT size (N)	1024
Cyclic prefix size (N_{cp})	$\frac{1}{4}N$
Number of data sub-carrier	234
Number of pilot	22
Oversampling factor (L)	4
Sub-carrier spacing	39.063 kHz
Symbol duration	1/39.063 kHz = 25.6 us
Number of symbol	7 (1 slot)
Filter type (N_f)	Kaiser,Hamming,Chebyshev,Blackman-Harris,Parks-McClellan
Filter order (N_f)	1500
Sampling frequency (f_s)	40 MHz
Modulation	4-QAM
Channel	AWGN

Different cutoff frequencies with the same ripple errors give different minimum filter orders as recorded in Table 3.2. It can be observed that the filter order is higher as the cutoff frequency is lower, where the transition bandwidth is narrower. Throughout this thesis, cutoff frequency of 5.06 MHz, which results in a reasonable passband value of 10.12 MHz, is considered. The number of sub-carriers in each given sub-band is 256, and typically one sub-band is obtained by the oversampling factor $L = 4$ to avoid aliasing. The parameters of OFDM system are the same as those of F-OFDM system, except that there is no filter applied.

TABLE 3.2: Passband Vs Filter Order

Passband(MHz)	**Filter Order**
10.24	750
10.16	1127
10.12	1500
10.08	2251
10.04	4500

As it can be seen from Figure 3.14, applying filter causes time delay in the resulting F-OFDM signal compared to the original OFDM signal. The delay caused by both transmitter filter and receiver filter is compensated with synchronization before removing CP at the receiver.

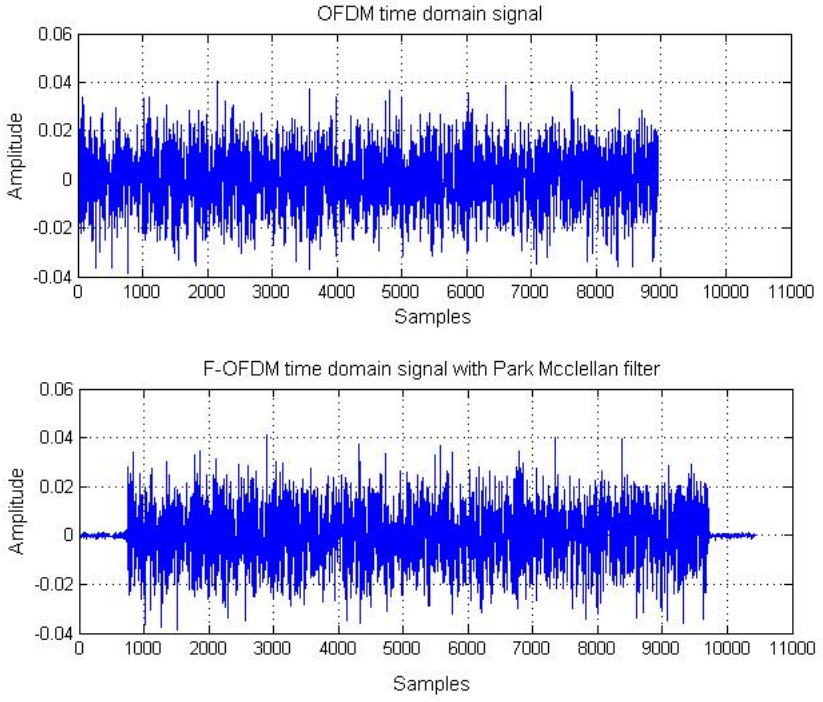

FIGURE 3.14: Time domain signal OFDM verse F-OFDM

Figure 3.15 illustrates the PSD comparison between conventional OFDM signal and F-OFDM signals with different filters. It can be clearly seen that the OOB emission level of F-OFDM signal is much lower than that of OFDM signal. Numerically, OOB emission of F-OFDM signal is 75 dB - 155 dB lower than the conventional OFDM signal. Blackman-Harris filter can obtain lower OOB emission approximately -190 dB

while Parks-McClellan filter can reach −200 dB. As discussed in the previous section, compared with the window based filter approach, Parks-McClellan filters can reach as lower OOB emission as desired by choosing smaller value of stopband ripple error, at the expense of higher filter order.

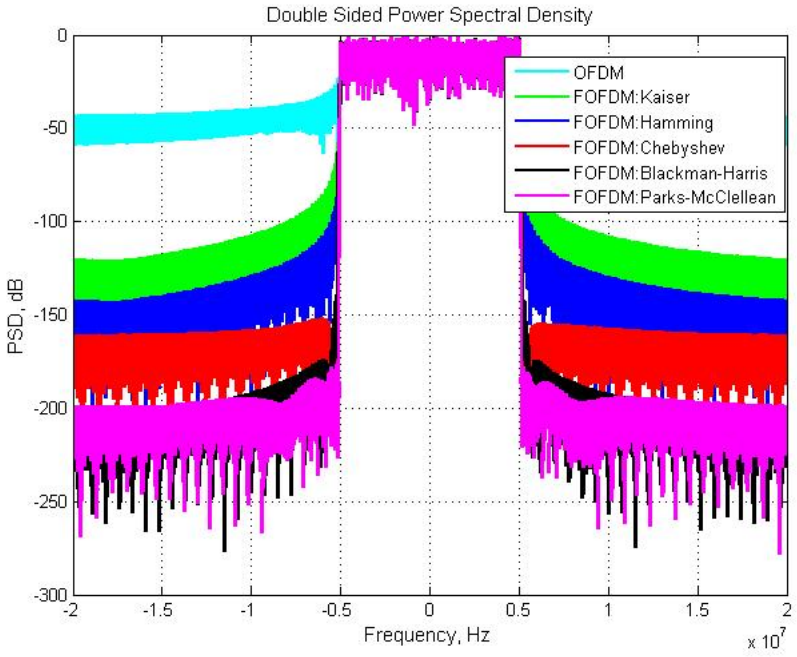

FIGURE 3.15: Normalized PSDs of OFDM and F-OFDM with different filters

Table 3.3 lists the PAPR values of the signals. The OFDM signal has the lowest PAPR values due to the fact that its OOB emission is very high. On the other hand, the F-OFDM signal with Parks-McClellan gives the highest PAPR. From the PAPR results, it can be said that in general the signals with lower OOB emission produce higher PAPR values. Higher PAPR is a disadvantage to a system with PA since it degrades the efficiency of the PA at the transmitter. The effect of PA on the F-OFDM signal will be demonstrated in the next chapter.

Table 3.3: PAPR values of F-OFDM signals

Signal	**PAPR(dB)**
OFDM	8.7016
F-OFDM(Kaiser)	10.1263
F-OFDM(Hamming)	10.1345
F-OFDM(Chebyshev)	10.1572
F-OFDM(Blackman-Harris)	10.1605
F-OFDM(Parks-McClellan)	10.4223

At the receiver, even though the wireless channel is AWGN, the effect caused by filters at both transmitter and receiver is compensated with equalizer. The constellation diagrams of the symbols recovered are shown in Figure 3.16. Due to the estimated channel(caused by AWGN and filters), the error between the transmitted and received symbols are large. Next, we will see the BER curves of the F-OFDM and OFDM signal. As plotted in Figure 3.17, BER simulation results of both OFDM and F-OFDM system are higher compared to the 4-QAM theoretical BER because of the CP energy. It can be seen that, at the higher signal to noise ratio, BER performance of F-OFDM signal with Parks-McClellan filter is the same as that of OFDM signal and slightly lower than that of both F-OFDM signal with Kaiser filter and Blackman-Harris filter. This is due to the fact that approximation error produced from windowing based filter is less accurate compared to Parks-McClellan filter.

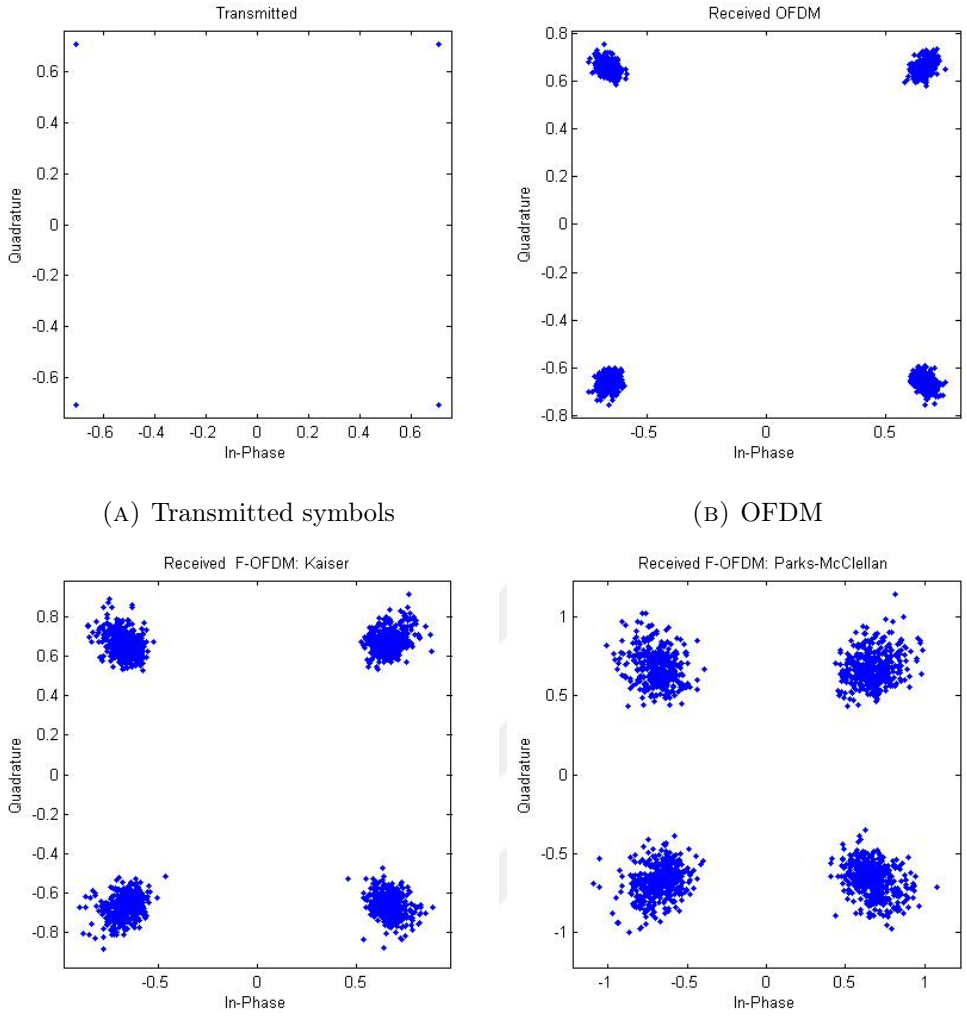

(A) Transmitted symbols

(B) OFDM

(C) F-OFDM:Kaiser

(D) F-OFDM:Parks-McClellan

FIGURE 3.16: Constellation diagram at SNR= 26 dB; (A) Transmitted symbols (B) Received OFDM (C)Received F-OFDM: Kaiser (D)Received F-OFDM: Parks-McClellan

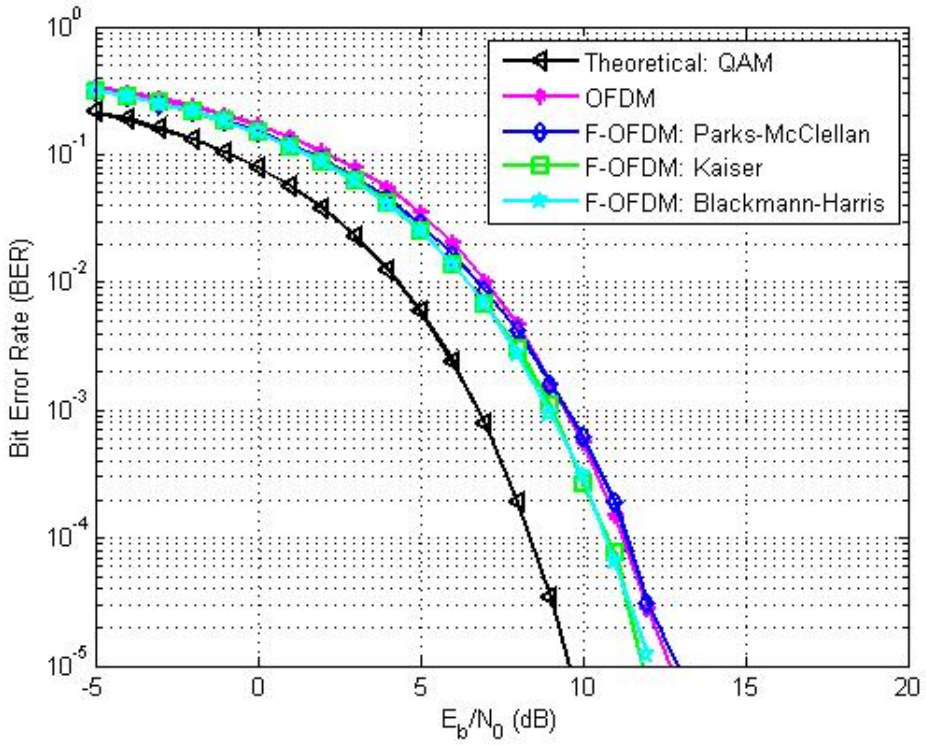

FIGURE 3.17: BER verse SNR graph of OFDM and F-OFDM

3.4 Conclusion

In this chapter, basic OFDM and F-OFDM systems were discussed. Then, filter designs of F-OFDM systems were elaborated. Lastly, performance comparison of OFDM and F-OFDM signals with different filters are accomplished. From the simulation results, in terms of PSD, lower OOB emission is achieved in F-OFDM signal with Parks-McClellan filter by using smaller value of stopband ripple. In addition to a lesser OOB emission, the F-OFDM signal with Parks-McClellan filter has the same BER performance with the OFDM signal. However, PAPR values of the F-OFDM signals are larger than that of the OFDM signal. Higher PAPR becomes a major disadvantage of the system when high PAs are employed. In the next chapter, the performance of F-OFDM system in the presence of the high PAs will be assessed.

Chapter 4

F-OFDM system with Pre-Distorter

In this chapter, the effect of HPA on F-OFDM signal will be firstly presented. In order to compensate the effect of the HPA, DPD is added in the system. Hence, pre-distortion based on memory polynomial will be discussed next. Lastly, simulation of F-OFDM system in the presence of both DPD and HPA will be performed and analyzed.

4.1 Effect of HPA on F-OFDM signal

In the previous chapter, performance of F-OFDM signal with a basic system was discussed. In the developed system, F-OFDM signal was transmitted right after passing it through a designed filter. However, here, HPA is applied at the transmitter-end to analyze the effect of amplifier on the F-OFDM signal. We will see that the behaviour of the F-OFDM signal changes after going through the amplifier. As discussed in Chapter 1, F-OFDM signal suffers from highly non-linear behaviour of the amplifier and hence, out of band emission becomes much higher.

The PA used in this study is a memory based PA with Saleh's model of traveling-wave tube (TWT) amplifier, which has a similar shape of the characteristics of solid state PA (SSPA). Amplitude to Amplitude (AM-AM) and Amplitude to Phase (AM-PM) transformation of Saleh's model PA is described as [37]:

$$A(x) = \frac{a|x|}{1 + b|x|^2} \quad \text{and} \quad \Delta\phi(x) = \frac{c|x|^2}{1 + d|x|^2} \tag{4.1}$$

where a, b, c and d are constant parameters of the PA, and the PA response is written as:

$$R(x) = A(x)e^{j(\phi_0 + \Delta\phi(x))} \tag{4.2}$$

where ϕ_0 denotes the phase of the input signal, x.

Saleh's model amplifier is memoryless, hence, in this study, memory effects are added based on the Hammerstein model [27][38][39]. As shown in Figure 4.1, the Hammerstein model amplifier is described as a conventional memoryless amplifier followed by a LTI system. Hammerstein model is one of the special cases of Volterra serie [27],[38]. Mathematically, the output of the Hammerstein model can be represented as [27]:

$$y(n) = \sum_{m=0}^{M-1} h_m \sum_{\substack{k=0 \\ k \text{ odd}}}^{K} g_k x(n-m)|x(n-m)|^{k-1} \tag{4.3}$$

where h_m are the impulse response values of the LTI system and g_k are the coefficients of the odd-order polynomial for the conventional memoryless system. In this case, as for the conventional memoryless amplifier, Saleh's model amplifier is applied, and as for LTI system, FIR low pass filter with 3 taps delay is adopted.

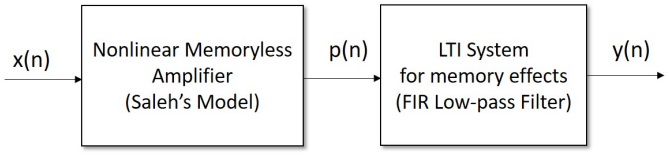

FIGURE 4.1: The Hammerstein model amplifier

Figure 4.2 shows the AM/AM curves of F-OFDM signal with memoryless PA and memory PA. It can be clearly seen from the curve with memory PA, due the memory effect, the same input sample eventually generates different output samples.

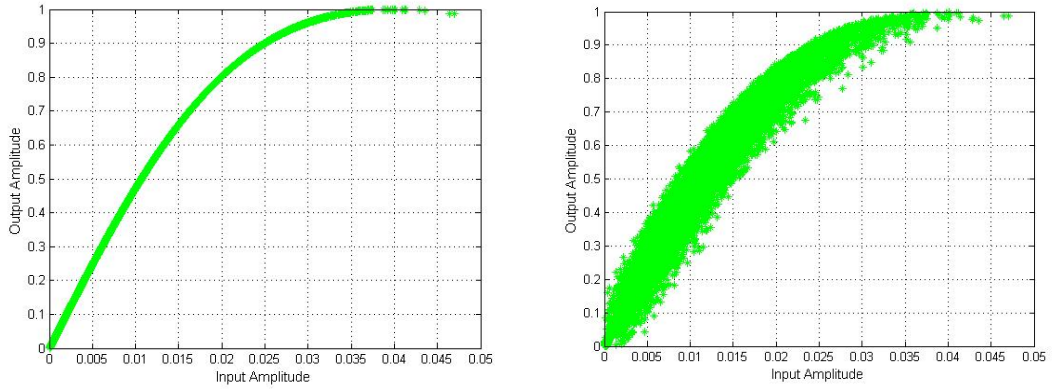

(A) AM-AM Curves of memoryless PA (B) AM-AM Curves of memory PA

FIGURE 4.2: AM-AM Curves of F-OFDM signal with (A)memoryless PA, (B)memory PA

If the PA is linear, output will be amplified with a linear gain. However, due to the non-linearity and memory effect of the PA as seen in Figure 4.2, the output signal does not get amplified linearly, resulting in amplitude distortion on received symbols as shown in Figure 4.3. Due to the filters, the constellation points in Figure 4.3a have small amplitude distortions. On the other hand, the constellation points in Figure 4.3b are amplified, yet they disperse a lot, resulting in bad BER performance.

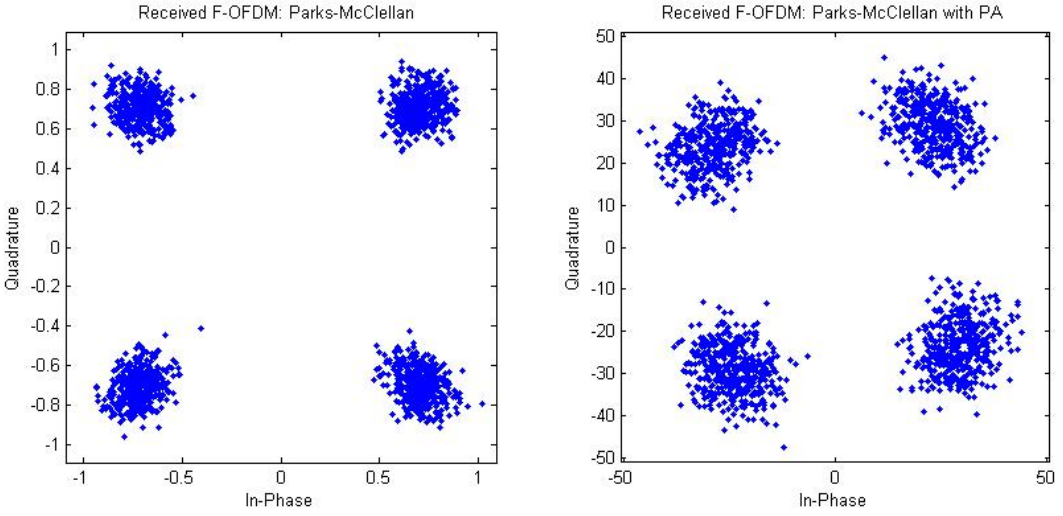

(A) Without PA (B) With PA

FIGURE 4.3: Constellation diagram of received symbols

Moreover, as exhibited in Figure 4.4, the amplitude of the zero padded subcarriers outside the bandwidth regrows after the signal has passed through the PA, hence, spectrum

efficiency is degraded. From the PSD graph shown in Figure 9, it is also observed that the OOB emissions level of f-OFDM signal in the presence of PA rises dramatically. For instance, the PSD value of f-OFDM with PA increases by about 170 dB at $\pm 10MHz$. However, even in the presence of the PA, F-OFDM signal has slightly lower OOB emission than that of OFDM signal as depicted in Figure 4.6. Due to the non-linear effect of the PA which causes both out-band and amplitude distortions, pre-distorter is implemented in the system and discussed in the following sections.

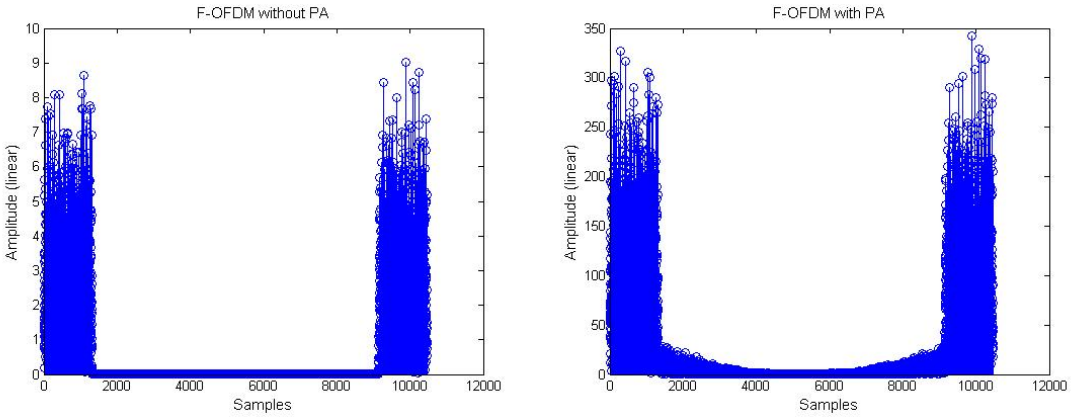

(A) Without PA (B) With PA

FIGURE 4.4: F-OFDM sub-carriers (A)without PA, (B)with PA

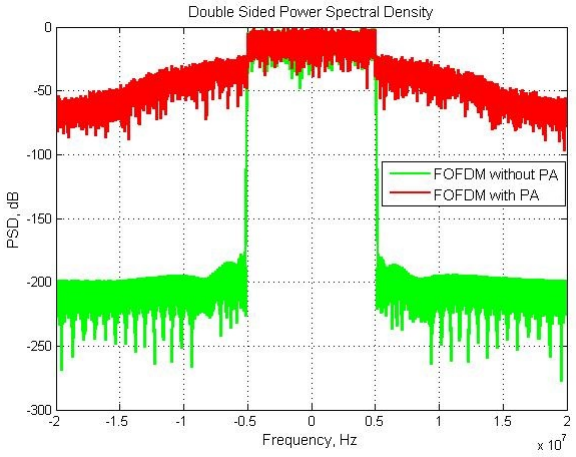

FIGURE 4.5: PSD of F-OFDM signal

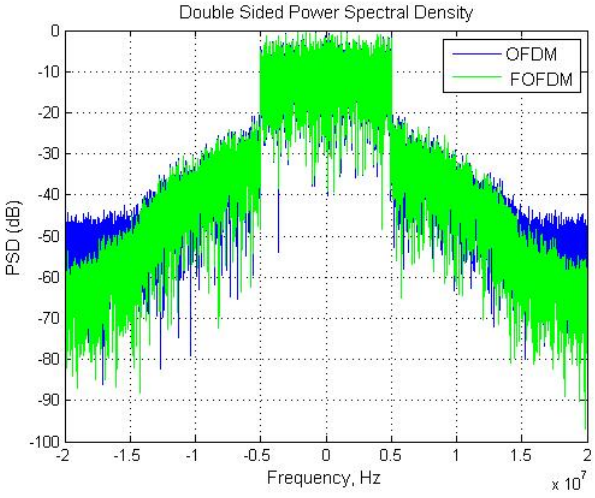

FIGURE 4.6: PSD of F-OFDM and OFDM signals in the presence of conventional PA

4.2 Implementing Digital Pre-Distortion

Pre-distortion is a process of applying an inverse non-linear function of a given PA on a signal prior to amplification. A predistorter has an inverse function of a PA response so that the input and output signals of the resulting block (predistorter + PA) are related linearly. Cascading the pre-distorter before PA should result in linear behavior of the output signal as Figure 4.7. In this study, a digital pre-distortion is developed by using the Memory Polynomial (MP) model and indirect learning architecture discussed in [10].

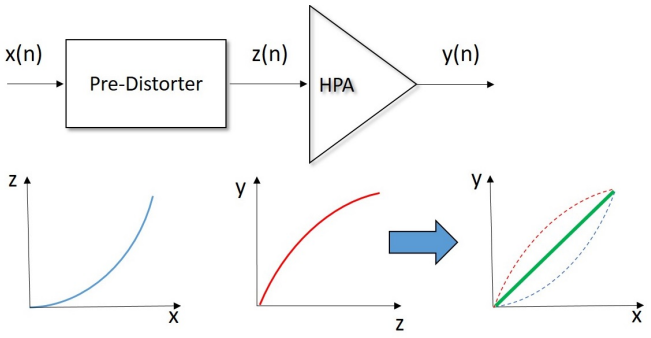

FIGURE 4.7: Pre-distortion effect on a given PA

4.2.1 Indirect Learning Architecture

There are two methods to construct the pre-distorter with memory: direct learning method and indirect learning method. In direct learning architecture, behavior of the

PA is firstly identified and then inverse of the PA is obtained [40]. However, due to the high complexity of finding the inverse of the non-linear system with memory, direct learning method is not preferable. On the other hand, in indirect learning architecture, the pre-distorter is constructed directly without requiring to determine the model of the PA.

Figure 4.8 illustrates the indirect learning structure. Before applying the pre-distorter, the output of the PA is normalized and sent to the "Predistorter Training" (block A) as $\frac{y(n)}{G}$, where G is the desired amplifier gain, and $\hat{z}(n)$ is generated from the training block. The function of the training block is to estimate the parameters of the actual pre-distorter by comparing $\hat{z}(n)$ with the actual pre-distorter output, $z(n)$. In the ideal case, it is required to obtain $y(n) = Gx(n)$ by making the error between $\hat{z}(n)$ and $z(n)$, $e(n) = 0$. The algorithm converges when minimum error energy $||e(n)||^2$ is achieved. After the algorithm has converged, the actual pre-distorter is modeled as an exact copy of the "Predistorter Training" block.

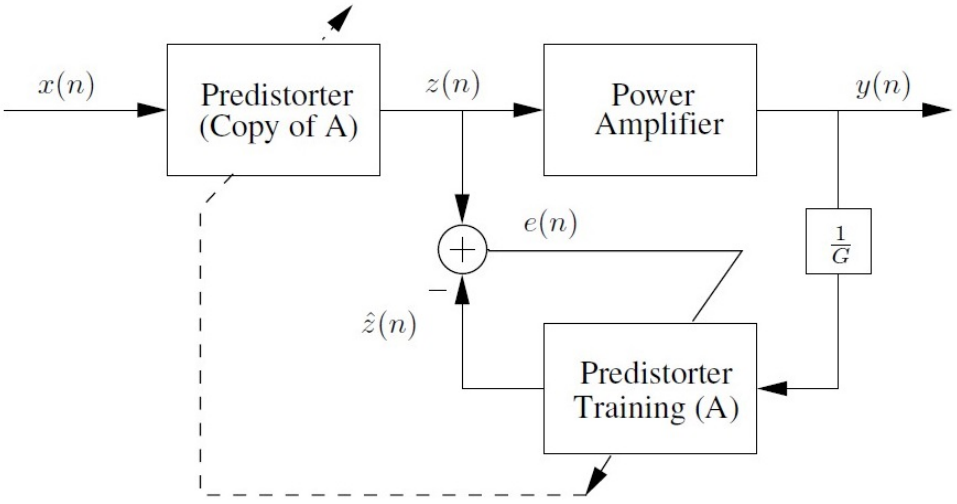

FIGURE 4.8: Indirect learning structure for the pre-distorter [10].

4.2.2 Coefficient Estimation of Memory Polynomial (MP) Pre-Distorter

The MP model is a generalizied form of the Hammerstein model. The pre-distortor based on MP model is formulated mathematically as [10]:

$$z(n) = \sum_{k=0}^{K-1} \sum_{m=0}^{M-1} d_{km} x(n-m)|x(n-m)|^k \tag{4.4}$$

where d_{km} are coefficients of the pre-distorter, and K and M are polynomial order and memory length of the pre-distorter respectively.

As discussed in the previous section, estimation of the coefficients of the pre-distorter is done by minimizing squared error. This method is known as a least squares (LS) estimation. With memory polynomial model, output of the PA before applying pre-distortion is obtained as:

$$y(n) = \sum_{k=0}^{K-1} \sum_{m=0}^{M-1} p_{km} x(n-m)|x(n-m)|^k \tag{4.5}$$

where p_{km} are coefficients of the memory based PA. As the training block in Figure 4.9 produces an inverse function of the PA, output of the pre-distorter training block, which is also the input of the PA, can be expressed as:

$$z(n) = \sum_{k=0}^{K-1} \sum_{m=0}^{M-1} d_{km} y_{norm}(n-m)|y_{norm}(n-m)|^k \tag{4.6}$$

where $y_{norm} = y/G$ is a normalized output of the PA before applying pre-distorter in the system. Given $y_{norm}(n)$ and $x(n)$, the Equation 4.6 can be rewritten as Equation 4.7, which is a matrix form to implement it in least squares estimation formula. That is,

$$\boldsymbol{z} = \boldsymbol{Y}\boldsymbol{d} \tag{4.7}$$

where

$$\begin{aligned}
\boldsymbol{z} &= [z(0), z(1), \cdots, z(N-1)]^{\mathrm{T}}, \quad \boldsymbol{z}_{N\times 1} \\
\boldsymbol{d} &= [d_{1,0}, \cdots, d_{K-1,0}, d_{1,1}, \cdots, d_{K-1,M-1}]^{\mathrm{T}}, \quad \boldsymbol{d}_{KM\times 1} \\
\boldsymbol{Y} &= [\boldsymbol{y}_{1,0}, \cdots, \boldsymbol{y}_{K-1,0}, \boldsymbol{y}_{1,1}, \cdots, \boldsymbol{y}_{K-1,M-1}], \quad \boldsymbol{Y}_{N\times KM} \\
\boldsymbol{y}_{k,m} &= [y_{k,m}(0), \cdots, d_{k,m}(N-1)]^{\mathrm{T}}, \quad \boldsymbol{y}_{k,m\,N\times 1}
\end{aligned}$$

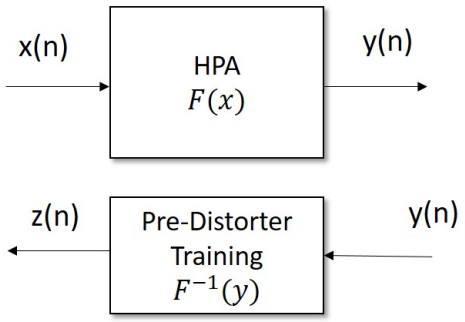

FIGURE 4.9: Pre-distorter as an inverse function of PA

By using the least squares estimation method, the coefficient vector $\boldsymbol{d}$ can be estimated as [41]:

$$\hat{\boldsymbol{d}} = (\boldsymbol{Y}^H \boldsymbol{Y})^{-1} \boldsymbol{Y}^H \boldsymbol{z} \tag{4.8}$$

where $(.)^H$ indicates complex conjugate transpose. The details of the memory polynomial pre-distorter algorithm is described in Figure 4.10.

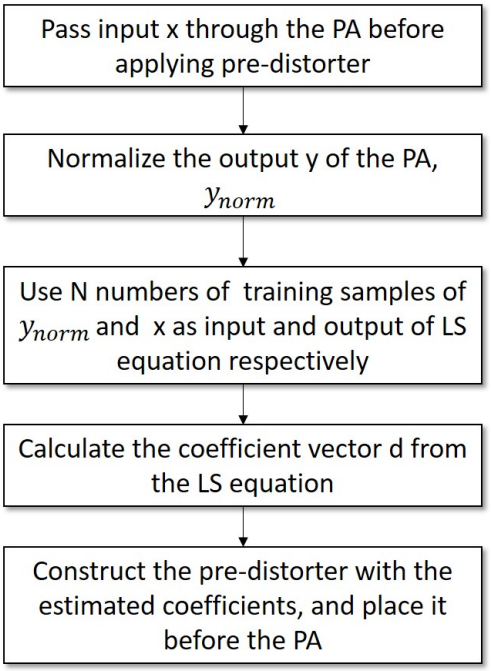

FIGURE 4.10: Flow chart of pre-distorter construction

4.2.3 Normalization Gain

In order to model the accurate inverse function of the PA without considering the effect of the amplifier gain on the amplifier output, it is required to normalize the output

response of the PA [42]. However, choosing proper normalization gain which is required to use in the accurate estimation of pre-distorter coefficients is one of the problems in implementing pre-distortion technique.

Different normalized gain selections have been applied in many studies. In [43], maximum gain of the linear region of the PA is used. However, it is not suitable to use this normalized gain in highly non-linear amplifier or wide-band signals with high PAPR such as F-OFDM signal. This due to the fact that the linear region is not wide enough to amplify the maximum input of the signal without distortion. As it can be seen in Figure 4.11, with the normalized gain of [43], the PA cannot operate in the saturation region, regarding the amplitude of the input signal at the saturation point as a maximum and neglecting all the amplitudes higher than the maximum.

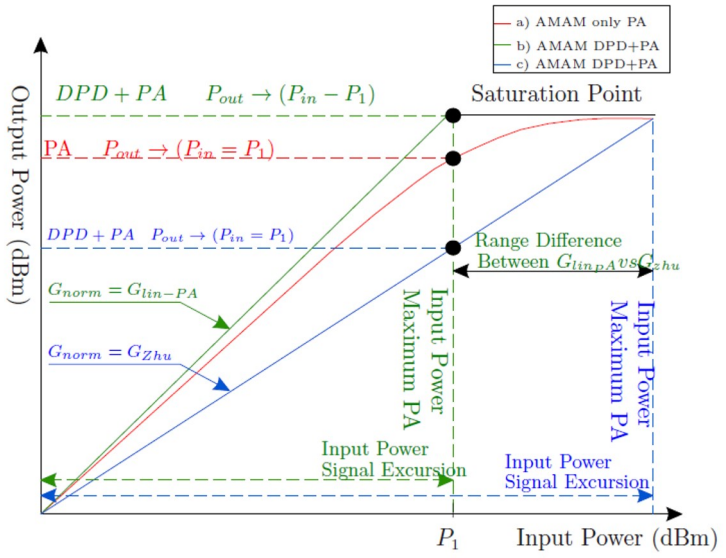

FIGURE 4.11: DPD with different normalized gain [11]

Even if there is no problem in choosing the maximum gain of the linear region (in the case of highly linear amplifier), this will cause the pre-distorted input and the original input of the PA to have different peak envelopes at the saturation point. Hence, different scaling factors are required to normalize the output and input of the PA in extracting the coefficients of DPD, which results in higher complexity of input power control when implementing the DPD-PA system [42].

Therefore, in [42], normalization gain based on maximum amplitude of the PA input and output was proposed as $G_{zhu} = max(output)/max(input)$. Moreover, it allows also

to amplify the signal with wide dynamic range and high PAPR. The downside of this selection is that the gain of the PA of the system is reduced in the final DPD-PA system.

The choice of the normalized gain depends not only on the property of the PA but also on the type of the transmitted signal. DPD with maximum gain in linearized region of PA used in [43] works only in the case of low PAPR signals while DPD with normalized gain, G_{zhu}, introduced in [42] works also for high PAPR signals [11].

4.3 Simulation and Analysis

In this section, performance of the F-OFDM system with the memory polynomial pre-distorter is demonstrated. F-OFDM signal is produced with Parks-McClellan filter by using the same simulation parameters used in Chapter 3 and the parameters listed in Table 4.1 for the PA and the pre-distorter. The constants of Saleh's model amplifier are selected to normalize both the input saturation amplitude, $A_{sat} = \frac{1}{\sqrt{b}}$, and the maximum output amplitude,$A_{max} = max(A(x)) = a\frac{A_{sat}}{2}$, to 1 and to obtain the saturation phase change, $\phi_{sat} = \phi(A_{sat}) = \frac{\pi}{12}$ [44].

TABLE 4.1: Parameters of PA and DPD

Parameter	Value
AM/AM constants of Saleh's Model	a=2, b=1
AM/PM constants of Saleh's Model	c=$\frac{\pi}{6}$, c=1
Input Gain, Output Gain	14 dB, 0 dB
Memory length (K)	3
non-linear order (M)	5
Normalization Gain	G_{zhu}
F-OFDM filter	Parks-McClellan

Pre-distorter with three memory and fifth order non-linearity is constructed by implementing the algorithm discussed in the previouse section. Since F-OFDM signal has a high PAPR, G_{zhu} is used to normalized the output of the PA in the algorithm. The

pre-distorter and the memory PA are added in the F-OFDM system as depicted in Figure 4.12.

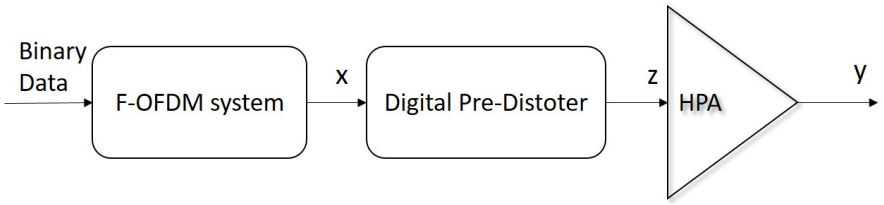

FIGURE 4.12: F-OFDM transmitter with DPD and PA

After applying pre-distorter in the system, the output of the conventional PA amplifies linearly as shown in Figure 4.13. Even though the behavior of the PA is linearized, due to the normalize gain used for the high PAPR signal, the PA gain is reduced.

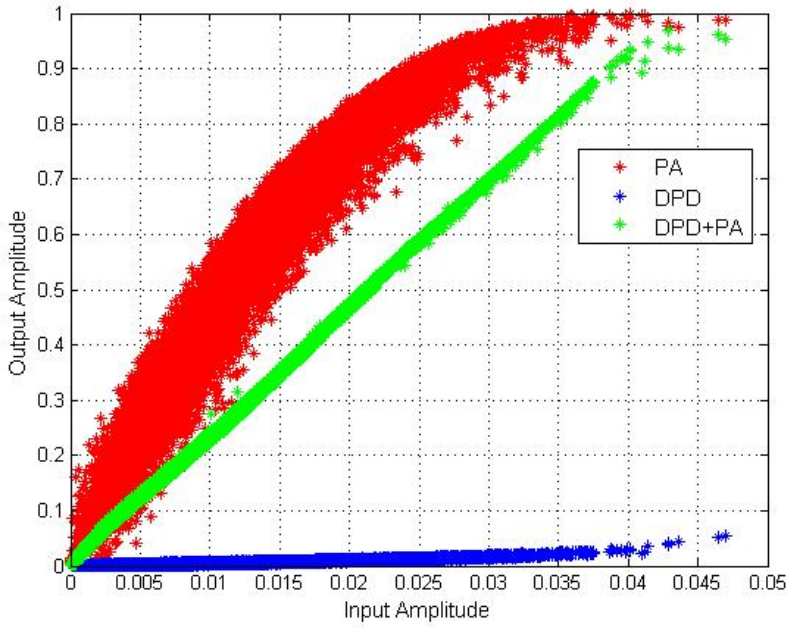

FIGURE 4.13: F-OFDM transmitter with DPD and PA

The power spectral density of the F-OFDM signal with and without pre-distorter is illustrated in Figure 4.14. It can be seen that with the pre-distorter, OOB emission is reduced by 10 dB. Thus, the spectral regrowth due to the conventional PA is suppressed fully.

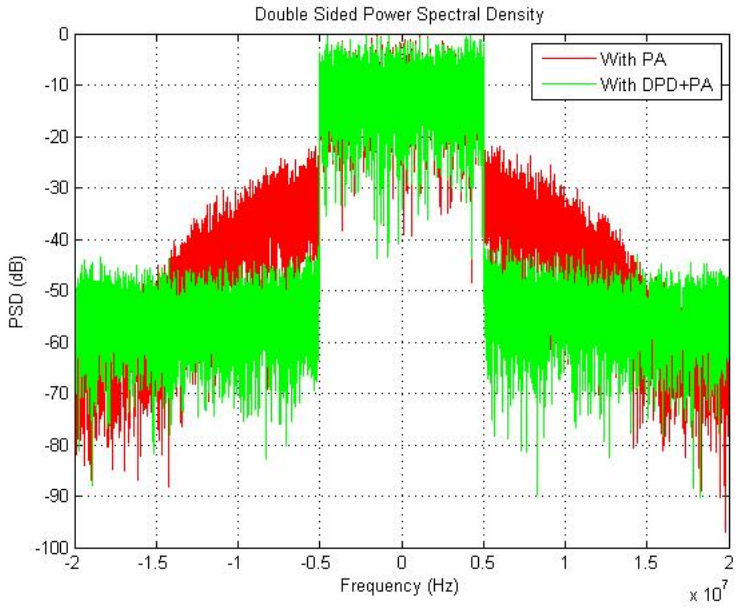

FIGURE 4.14: Power spectral density of F-OFDM signal with and without DPD

In addition to the ability to suppress the spectrum regrowth, the same BER performance of the original F-OFDM can also be achieved by applying the pre-distorter in the system. As it can be seen in Figure 4.15, BER performance deteriorates greatly in the presence of the conventional PA. After the PA is linearized with the pre-distorter, the BER performance improves and ultimately achieves the same performance as in the original F-OFDM system without the PA.

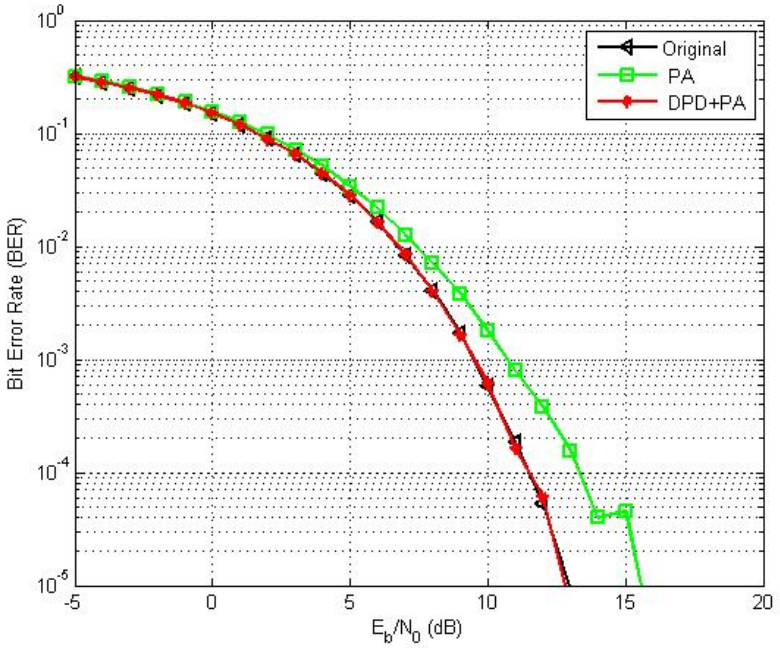

FIGURE 4.15: BER curve of F-OFDM signal with and without DPD

4.4 Conclusion

In this chapter, the effect of the conventional PA on the F-OFDM signal was demonstrated. Due the non-linear behavior of the PA, OOB spectrum of the F-OFDM signal regrows and BER performance is also degraded. Therefore, pre-distortion technique, which can compensate the non-linear behaviour of the PA, is discussed next. Due to the fact that F-OFDM signal is a wideband signal, which considers memory effect, memory based polynomial pre-distorter is applied in the system. Finally, simulation of the F-OFDM system with the pre-distortion and the PA was performed. From the simulation results, applying pre-distorter suppresses the OOB spectrum and also improves the BER performance compared to the system with only PA.

Chapter 5

F-OFDM system with Optimized ICF and Pre-Distorter

In this chapter, PAPR reducing technique based on optimized iterative clipping and filtering will be discussed first. The optimized ICF block is added in the F-OFDM system, and without using the pre-distorter, performance of the updated system in the presence of PA will be evaluated next. Finally, the performance of F-OFDM system with both optimized ICF and pre-distorter will be analyzed.

5.1 F-OFDM System with the Optimized ICF

F-OFDM systems provide much lower OOB emission than OFDM systems, but they still hold the disadvantages of OFDM systems such as high PAPR. In OFDM systems, coherent summation of independent subcarriers with different phase results in a peak amplitude much larger than the average amplitude of the transmitting signal [45] Similarly, F-OFDM systems also suffer from higher PAPR. ICF technique is commonly used to reduce PAPR due to its simplicity, yet it takes many iterations to achieve a desired PAPR [28]. The PAPR of the original time domain F-OFDM symbol, $\boldsymbol{x_0}$, is written as [28],

$$PAPR = \frac{\|\boldsymbol{x_0}\|_\infty^2}{\frac{1}{N}\|\boldsymbol{x_0}\|_2^2} \tag{5.1}$$

where $\|\cdot\|_\infty$ represents the $l^\infty - norm$, which is defined as peak envelope, and $\|\cdot\|_2$ is the $l^2 - norm$.

5.1.1 Conventional Iterative Clipping and Filtering

In conventional ICF technique, a time domain symbol, $x(k)$ is first clipped to a predefined clipping threshold; A, and then OOB spectrum is suppressed by rectangular window based filter. The time domain clipped F-OFDM symbol at m^{th} iteration; $\boldsymbol{x_c}^{[m]}(k)$, is obtained as [28]

$$\boldsymbol{x_c}^{[m]}(k) = \begin{cases} A^{[m]} e^{j\theta^{[m]}}(k), & |x^{[m]}(k)| > A^{[m]} \\ x^{[m]}(k), & |x^{[m]}(k)| \leq A^{[m]} \end{cases} \tag{5.2}$$

where $\theta^{[m]}$ is the phase of $\boldsymbol{x}^{[m]}(k)$. $A^{[m]}$ at m^{th} iteration is calculated from clipping ratio (CR) and root mean square of the time domain signal as follows [28]:

$$A^{[m]} = CR\sqrt{\frac{1}{N}}\|\boldsymbol{x}^{[m]}\| \tag{5.3}$$

Clipping the amplitude of the signals causes amplitude distortion in time domain and also spectrum spread in frequency domain. Therefore, in order to suppress the OOB spectrum, filtering process is required after clipping. Frequency response of the window based filter used in the conventional ICF is defined as [28]

$$H^{[m]}(q) = \begin{cases} 1, & 1 \leq q < N_{sub} \\ 0, & N_{sub} + 1 \leq q < N \end{cases} \tag{5.4}$$

The range between 1 and N_{sub} represents in-band component indices, and from $N_{sub}+1$ to N are out-band component indices. As it can be seen from the frequency response of $H^{[m]}(q)$, the filter lets all the in-band spectrum of the clipped signal pass and makes OOB components zero, which leads to peak regrowth in time domain. Hence, repetitive process of clipping and filtering requires many iterations until the PAPR reaches to the desired value.

5.1.2 Optimized Iterative Clipping and Filtering

Optimized ICF, by contrast, needs much lesser iterations to obtain the desired PAPR by considering the peak regrowth affected by filtering. Two parameters to be considered in optimizing the clipping and filtering are in band distortion, which can be measured

from error vector magnitude (EVM) between original sub-carriers, $\boldsymbol{d_{in0}}$ and in-band clipped and filtered sub-carriers, $\boldsymbol{d_{in}}$; and spectrum spread. Large EVM degrades the BER performance, and spectrum spread results in high OOB emission and interferes with the adjacent spectrum. The goal of this optimization is to obtain a sub-optimum filter by minimizing EVM while making OOB spectrum low with the resulting PAPR less than and equal to the desired PAPR. The optimization problem at m^{th} iteration can be written as a convex optimization formula as follows:

$$\underset{\boldsymbol{H}^{[m]} \in \mathbb{C}^N}{\text{minimize}} \quad EVM = \frac{\|\boldsymbol{d_{in0}} - \boldsymbol{d_{in}}^{[m]}\|_2}{\|\boldsymbol{d_{in0}}\|_2} \tag{5.5a}$$

$$\text{subject to} \quad \|W([\boldsymbol{d_{in}}_c^{[m]} \cdot \boldsymbol{H_{in}}^{[m]}; \boldsymbol{d_{out}}_c^{[m]} \cdot \boldsymbol{H_{out}}^{[m]}])\|_\infty \leq \sqrt{\frac{1}{N}} \|\boldsymbol{x_c}^{[m]}\|_2 \text{CR} \tag{5.5b}$$

EVM is measured between the in-band spectrum only since the data sub-carriers are located at the in-band spectrum. The equation 5.5b is a constraint to achieve the desired CR given as $CR = \sqrt{PAPR_{max}}$. Here, $\boldsymbol{H_{in}}^{[m]}$ and $\boldsymbol{H_{out}}^{[m]}$ are in-band and out-band frequency response vectors respectively, and W is N-point IFFT twiddle factor matrix. $\boldsymbol{d_{inc}}^{[m]}$ and $\boldsymbol{d_{outc}}^{[m]}$ are in-band and out-band spectrum vectors of the clipped F-OFDM symbol.

The equation 5.5 is adapted from the study done in [28]. When compared to the constraint used in [28], which considers only in-band spectrum components of the symbol in converting the frequency domain spectrum into the time domain symbol, in this modified method, out-band components are also taken into account. This is because out-band spectrum components of the original F-OFDM symbol are not zero due to the filtering process, which causes spectrum leakage. The optimized filter in [28] totally suppressed the out-band components, making them all zero. In contrast, in this method, we let out-band coefficients of the targeted filter equal to that of the undistorted out-band spectrum components, thus element-wise multiplication between them results in lower OOB spectrum without making it zero. At the end of the optimization step in each iteration, the clipped and filtered sub-carriers vector is obtained as $\boldsymbol{d}^{[m]} = [\boldsymbol{d_{in}}^{[m]}; \boldsymbol{d_{out}}^{[m]}]$.

The modified optimized ICF procedure for a single F-OFDM symbol, summarized below, is a modified version of the method introduced in [28].

1. Initialization Step: Set the CR threshold and maximum number of iterations, M.

2. At the first iteration m=1, converts the original signal vector $\boldsymbol{x_0}^{[m]}$ into frequency domain undistorted signal vector, $\boldsymbol{d_0} = [\boldsymbol{d_{in0}}; \boldsymbol{d_{out0}}]$ using FFT.

3. If m=1, let $\boldsymbol{x_0}^{[m]} = \boldsymbol{x_0}^{[m]}$, otherwise, $\boldsymbol{x_0}^{[m]} = \boldsymbol{x_0}^{[m-1]}$.

4. Clip $\boldsymbol{x_0}^{[m]}$ into $\boldsymbol{x_c}^{[m]}$ by using the equation 5.2 with $A^{[m]}$, calculated from the equation 5.3.

5. Transform $\boldsymbol{x_c}^{[m]}$ into $d_c{}^{[m]} = [\boldsymbol{d_{inc}}^{[m]}; \boldsymbol{d_{outc}}^{[m]}]$ using FFT.

6. Set $\boldsymbol{H_{out}}^{[m]} = \boldsymbol{d_{out0}}$, and obtain $\boldsymbol{H_{in}}^{[m]}$ by performing the optimization step in 5.5.

7. Generate the sub-optimized clipped and filtered signal $\boldsymbol{x}^{[m]}$ by multiplying $\boldsymbol{d_c}^{[m]}$ with $\boldsymbol{H}^{[m]} = [\boldsymbol{H_{in}}^{[m]}; \boldsymbol{H_{out}}^{[m]}]$ and then, applying IFFT.

8. Increase $m = m + 1$, and repeat the process from step 3 until $m = M$. And then, repeat the whole procedure for the next F-OFDM symbol.

5.2 Simulation and Analysis

In this section, simulations of the following F-OFDM systems are performed:

1. F-OFDM system with the modified optimized ICF

2. F-OFDM system with both the pre-distorter and the optimized ICF

A F-OFDM signal is produced from one OFDM symbol with the same simulation parameters listed in Tabel 3.1. As for the filter, Parks-McClellan filter with stopband ripple peak of 10^{-6}, which results in filter order of 1140. The optimization was done in MATLAB with *CVX* package [46].

5.2.1 F-OFDM System with the modified Optimized ICF

F-OFDM system integrated with the modified optimized ICF technique will be simulated first. Without any PAPR reducing technique or PA distortion, the F-OFDM signal gives high PAPR value, 11.0581 dB numerically. Hence, iterative clipping and filtering with

$CR = \sqrt{3.162} = 1.7783$ [28], is performed on the signal to reduce the PAPR up to 5 dB (3.162).

Firstly, the effect of the conventional ICF (Armstrong method) on the F-OFDM signal will be presented. Figure 5.1 shows the clipping effect on the F-OFDM symbol. It can be observed that after clipping is performed in time domain, the amplitude of the time domain F-OFDM symbol is cut into a pre-defined amplitude level according to the clipping ratio.

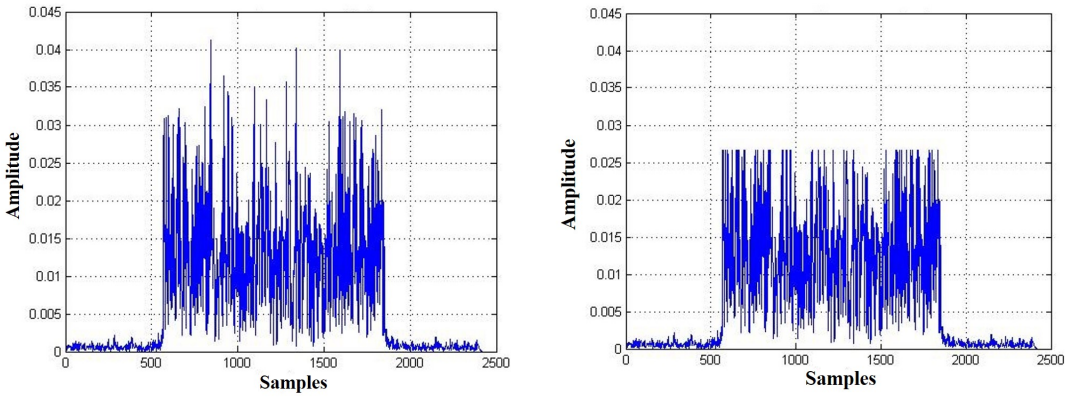

(A) Before clipping (B) After clipping

FIGURE 5.1: Time domain F-OFDM signal (A) before clipping, (B) after clipping

While the PAPR value is reduced to 3.9192 dB, the OOB components of the frequency domain symbol gain some values, as shown in Figure 5.2, resulting in the increased OOB emission. Therefore, ideal rectangular low pass filter is used to cancel the out-band components completely without affecting the in-band components. However, it causes the peak regrowth in the resulting time domain symbol, leading to larger PAPR.

Figure 5.3 compares the time domain F-OFDM symbol before and after applying the low pass filter on the clipped symbol. It can be seen that the amplitude of the clipped and filtered signal exceeds the peak amplitude of the clipped signal, hence, the PAPR becomes higher and is recorded as 8.4873 dB. This is for one iteration only, with 12 iterations, the PAPR reaches to 5.5179 dB, which is close to the maximum PAPR desired.

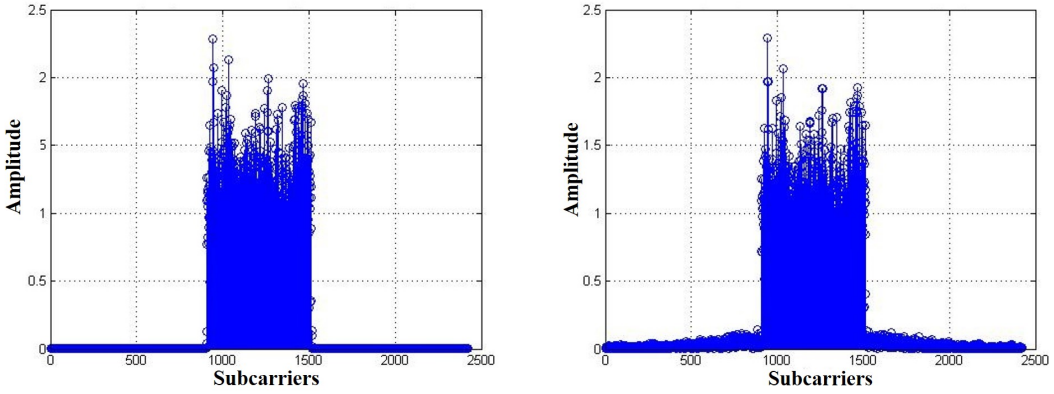

(A) Before clipping (B) After clipping

FIGURE 5.2: Frequency domain F-OFDM signal (A) before clipping, (B) after clipping

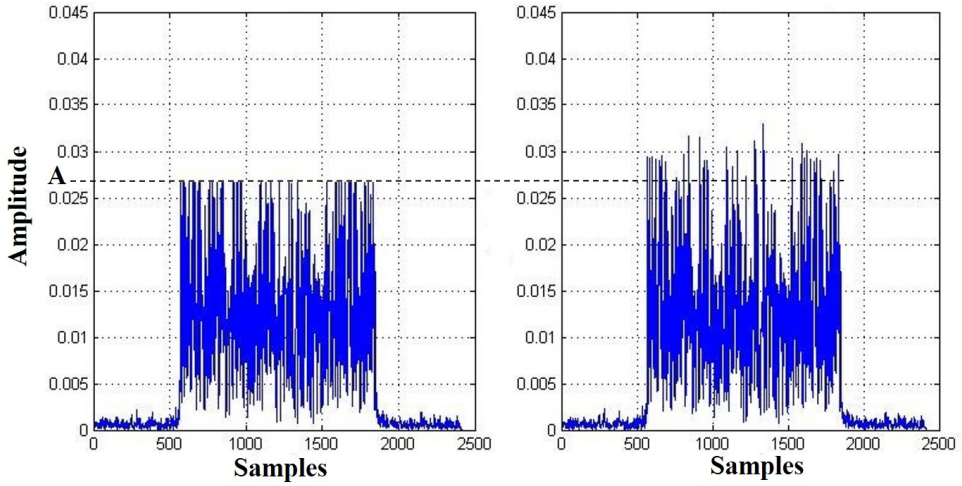

FIGURE 5.3: A comparison between clipped signal and clipped and filtered signal

On the other hand, optimized ICF method can greatly reduce the PAPR after a few iterations. The PAPR values obtained from the method used in this thesis and the method proposed in [28] and are recorded in Table 5.1. With the original method, the PAPR is dropped to 6.0509 dB after only one iteration and to 5.5117 dB after two iterations. Compared to the original approach, the modified method can reduces the PAPR to lesser value; 5.5067 dB after two iterations.

TABLE 5.1: PAPR values of original optimized ICF method [28] and the modified method

Method	PAPR(dB) Iteration=1	PAPR(dB) Iteration=2
Original method	6.0509	5.5117
Modified method	6.0585	5.5067

Figure 5.3 compares amplitude of the signal resulting from the modified optimized ICF method with that of Armstrong method after 1 iteration. It is shown that while the Armstrong filter makes the amplitude of the clipped signal regrow, the optimized filtering mitigates the regrowth.

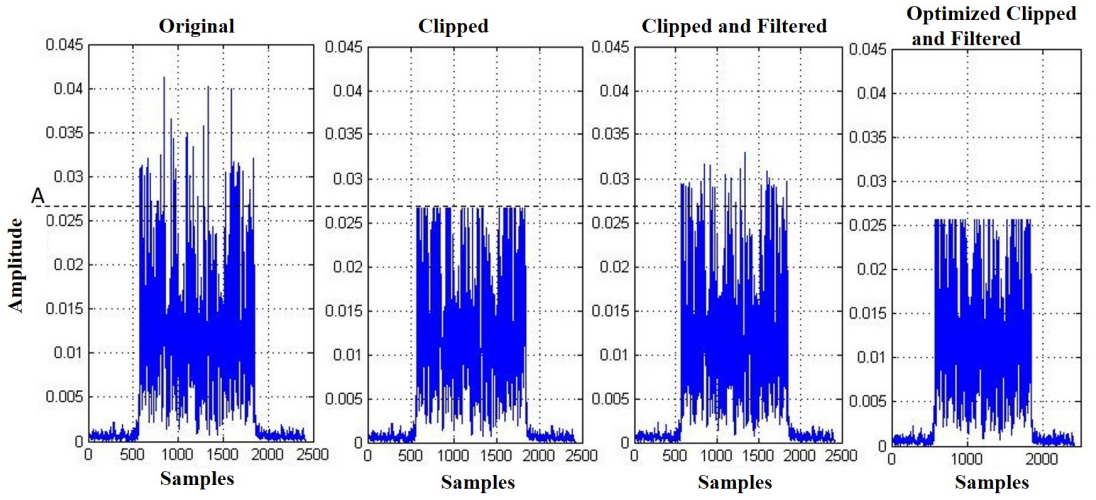

FIGURE 5.4: Time domain F-OFDM with Armstrong method and modified optimized ICF method after 1 iteration

Frequency responses of Armstrong method and the optimized method after 2 iterations are shown in Figure 5.5. It can be seen that in the optimized method, there is amplitude fluctuation while the amplitude of Armstrong method is always constant in passband. This variation in pass-band amplitude is a result of the optimization to prevent the amplitude regrowth in time domain.

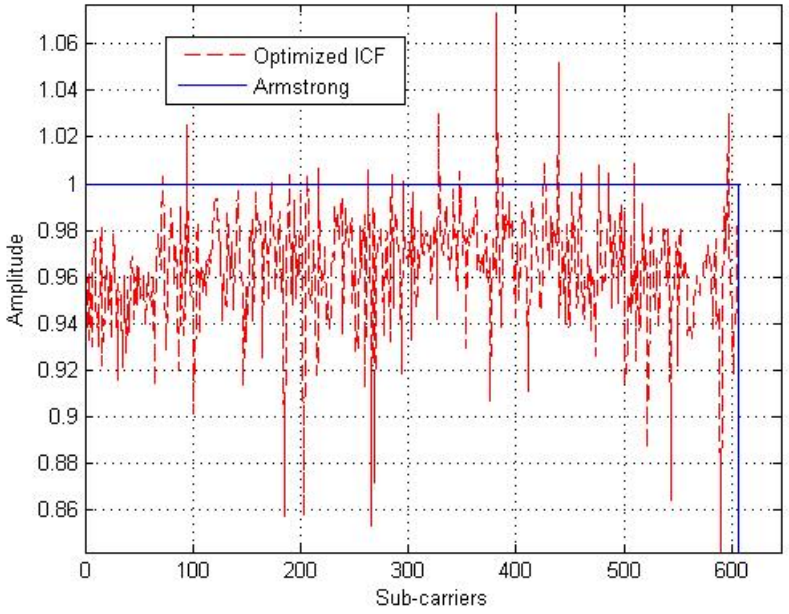

FIGURE 5.5: Frequency response comparison of optimized filter after 2 iteration with Armstrong filter

After processing the PAPR reducing technique, the resulting signals are passed through the conventional PA with the parameters described in Table 4.1 in Chapter 4, without applying the pre-distorter. Figure 5.6 plots the PSD of unprocessed F-OFDM signal, with Armstrong filter after 12 iterations and the optimized ICF after 2 iterations. It is observed that OOB power spectrum of both methods are reduced to about 9 dB lower than that of the unmodified signal at ± 10 MHz.

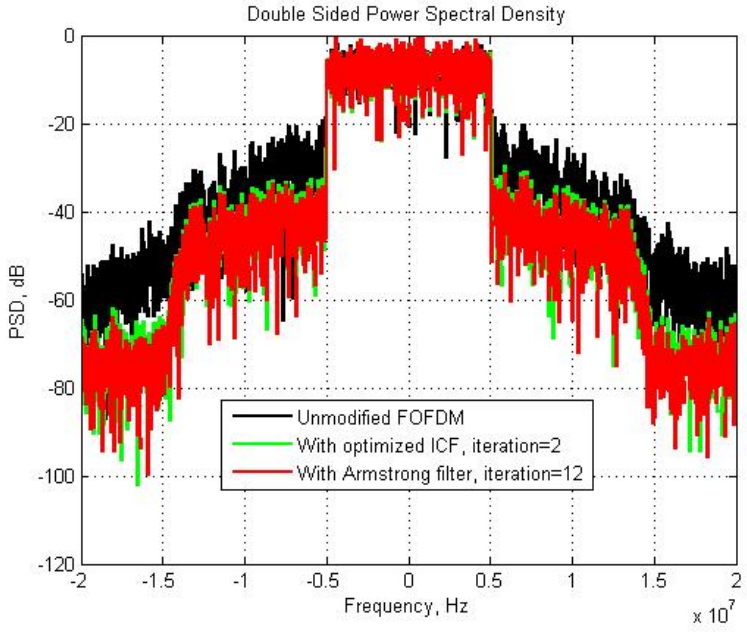

FIGURE 5.6: PSD of F-OFDM using optimized ICF after 2 iterations and Armstrong method after 12 iterations

Figure 5.7 presents the BER performance of the original F-OFDM signal without and with PA; and the modified signal with PA using the original optimized ICF (2 iterations), the modified optimized ICF (2 iterations) and Armstrong method (12 iterations). It is obvious that the BER performance degrades significantly after applying the clipping and filter methods. This is due to the fact that clipping process cuts peak amplitudes of the original signal, resulting in signal distortion. From the observation of the BER curves, compared to Armstrong method, the optimized ICF methods produces smaller BER at the high SNR values, specifically the modified optimized ICF perform the best among all the ICF methods by yielding a BER of $\log_{10}(\frac{1}{8} \times 10^{-2})$ at a SNR value of 20 dB. Thus, it is evident that the optimized methods cause lesser signal distortion and need fewer iterations than Armstrong method.

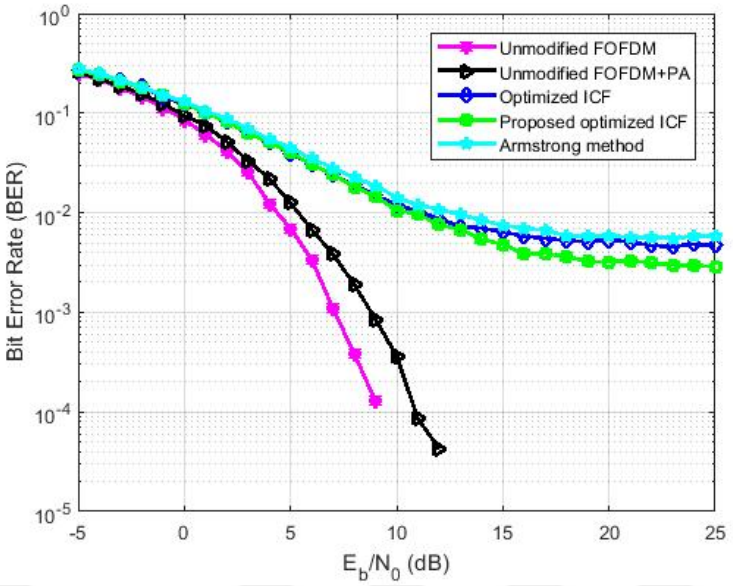

FIGURE 5.7: BER comparison between optimized ICF after 2 iterations and Armstrong method after 12 iterations

5.2.2 F-OFDM System with both the Pre-Distorter and the Optimized ICF

In this section, the performance of F-OFDM system consisting of Optimized ICF block and DPD block will be analyzed. Optimized ICF block is added in the system as shown in the system model in Figure 5.8. Here, we will discuss the simulation results obtained from the system with 1 iteration of the Optimized ICF.

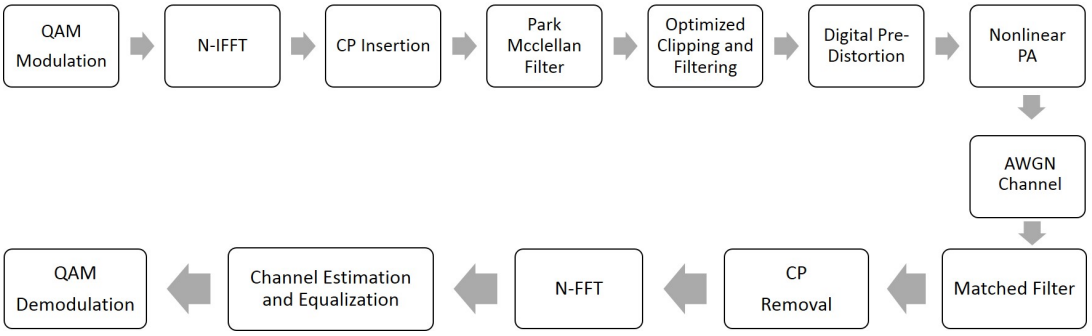

FIGURE 5.8: Complete system model for F-OFDM system

Figure 5.9 compares the PSD of optimized F-OFDM with and without DPD. It can be seen that the OOB spectrum regrowth is totally suppressed after applying DPD. It is also observed that compared to unmodified F-OFDM signal, F-OFDM, the OOB emissions

of the optimized signal are obviously reduced. For example, at the frequency of ±10 MHz, the combined method yields OOB emission level about 10 dB lower than just the optimized ICF method without pre-distortion.

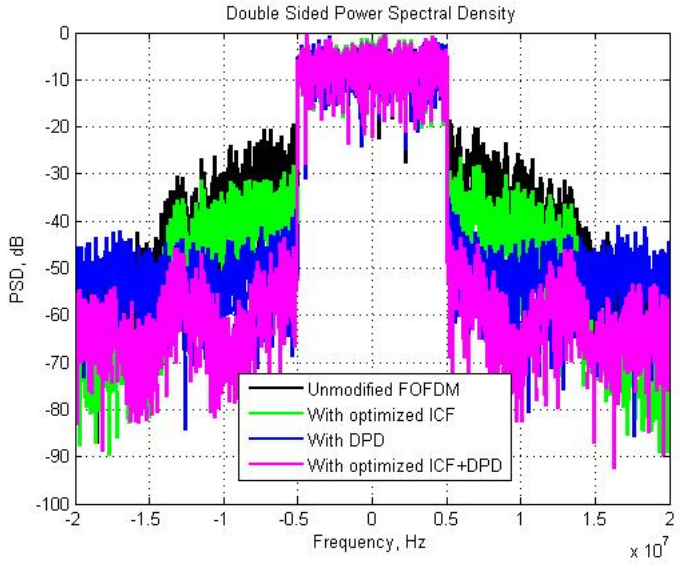

FIGURE 5.9: PSD comparison of optimized F-OFDM signal with and without DPD, 1 iteration

Next, we will compare the BER performance between optimized F-OFDM signal with and without DPD in the presence of the conventional PA. As depicted in Figure 5.10, BER of the optimized F-OFDM with DPD outperforms the BER of the system without DPD. As it can seen, compared to the BER of the original signal, the BER of the optimized signal is higher, which is the effect of clipping to reduce the PAPR. Hence, it can be said that there is a trade-off between the PAPR and the BER performance.

While including the cascaded block of optimized ICF and DPD mitigates the effect non-linear PA by increasing BER performance and reducing OOB emisison, the complexity of the system increases. In the worst case, the computational complexity to solve the second-order cone programming model of the optimization in equation 5.5 is $O(N^3)$ [47]. The complexity of the DPD depends on the polynomial degree and the memory length, and it requires to estimate KM numbers of coefficient.

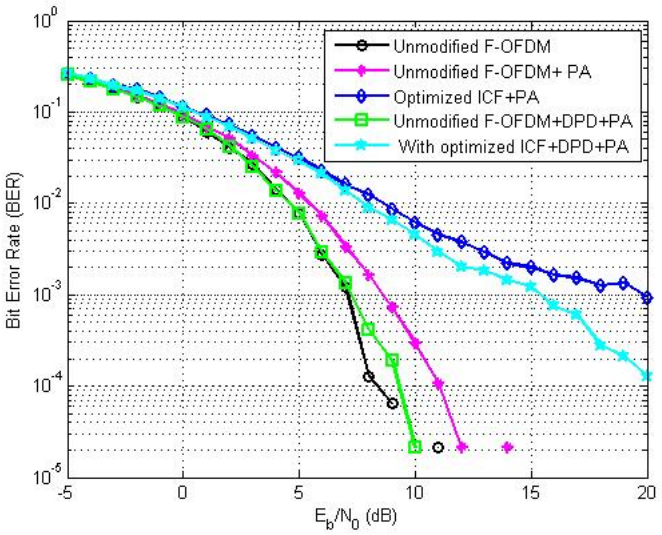

FIGURE 5.10: BER comparison of optimized F-OFDM signal with and without DPD, 1 iteration

5.3 Conclusion

In this chapter, the classical approach in ICF and the optimized ICF were elaborated mathematically. Then, the performance of the F-OFDM system consisted of optimized ICF without DPD was compared with the convention ICF (Armstrong method). From the observation, the optimized method requires lesser iterations than Armstrong method to achieve similar performance in terms of PSD and BER. Lastly, F-OFDM system with the optimized ICF and the pre-distortion was simulated. It is evident that OOB spectrum regrowth caused by the conventional PA is suppressed by using DPD in both the unmodified F-OFDM and the optimized F-OFDM. Moreover, by comparing the optimized F-OFDM signals with and without DPD, it was shown that DPD makes the BER performance of the optimized F-OFDM signal much better. On the other hand, in the case of the original signal and the optimized signal, in the presence of DPD, it was observed that optimized signal leads to much lower OOB emission than the original signal while its BER performance was degraded due to the clipping effect. It can be concluded that optimizing the F-OFDM signal has lower OOB emission as an advantage and larger BER values as a drawback.

Chapter 6

Conclusion

6.1 Summary

The thesis presented the performance evaluation of F-OFDM system in the presence of the conventional PA. F-OFDM scheme is one of the waveform candidates for the future wireless communication generation 5G. It is based on the classical OFDM system with sub-band based filtering. 5G is expected to provide much larger bandwidth, and F-OFDM will utilize the large bandwidth efficiently by dividing it into the several sub-bands, which can be allocated for different types of services. Due to the sub-band based filtering, asynchronous transmission can be done without the need of and OOB emission is reduced, resulting in smaller guard band.

The major process in F-OFDM is designing an appropriate filter, which can mitigate OOB spectrum emission while letting all in-band spectrum pass. We discussed the performance of F-OFDM signal generated with different filtering methods. Here, windowing-based filter and optimized filter by Parks-McClellan were compared in terms of PSD and BER performance. It is shown that much lower OOB spectrum can be achieved by using Parks-McClellan filter with smaller stopband ripple values at the expense of higher filter order. Moreover, its BER performance is also similar to OFDM signal. All the simulations done in this study were with AWGN channel.

Even though F-OFDM provide a reduced OOB emission, it has a higher PAPR than OFDM. In the presence of the conventional PA, the high PAPR signal will result in non-linear distortion in time domain and also will increase OOB spectrum in frequency

domain. Therefore, PA linearization method was also employed in the F-OFDM system. Pre-distorting technique was used since it is the easiest method to linearize the non-linear behavior of the PA. Here, F-OFDM is the wide-band signal, hence, memory effects are needed to be considered when implementing the pre-distorter. Simulation results show that pre-distortion suppresses the spectrum regrowth in OOB frequencies while improving BER performance.

Another method to reduce the OOB emission caused by PAPR is PAPR reducing technique. We compared the classical PAPR reducing technique obtained from two approaches: the optimized ICF and the conventional ICF. Simulations were firstly performed without the presence of DPD, in order to analyze the effect of the ICF alone on the signal. It is shown that the conventional ICF is simple but it needs many iterations to achieve the desired PAPR values while the optimized method needs only a few iterations. After performing the simulation of the F-OFDM system only with the PAPR reducing technique, next, pre-distortion was also added in the system and the overall system was analyzed. It is observed that, without DPD, it is not possible to suppress the OOB spectrum regrowth caused by PAPR even though optimized ICF is present. The advantage of having optimized ICF in the system along with the DPD is that it achieves much lower OOB emission in contrast to the system with only DPD. The side effect of optimized ICF is the distortion caused by clipping, hence, BER performance is worse than without applying the PAPR reducing technique.

With all the work performed in this study, the techniques used in OFDM system to mitigate the effect of the conventional PA are applied in F-OFDM system. It can be concluded that in the presence of the PA, the performance of F-OFDM system is greatly reduced in terms of OOB emission and BER. By deploying the same techniques used to suppress the PA effects in OFDM, the performance of F-OFDM is improved, however, OOB emission of F-OFDM signal does not get reduced to the initial OOB emission level of the signal transmitted without the PA.

In this thesis, performance of the F-OFDM system was discussed, and the numerical results were shown step by step throughout the discussion. Apart from the basis F-OFDM system with different filter designs, which is mostly done in many literature, the conventional PA was also included in the system in order to give clear understanding of the PA's

effect on the F-OFDM signal. Moreover, to mitigate the effect of the PA, PAPR reducing technique (optimized ICF) and PA linearization technique (pre-disortion) employed in 4G OFDM system was also applied in the F-OFDM system and their performance were compared. We conclude that the combined technique of the optimized ICF and the predistortion helps improve both OOB and BER performance of F-OFDM system in the presence of nonlinear PA when compared to a system with no predistorter. Therefore, the combined technique is a significant part of the F-OFDM system in 5G to fully utilize the benefits of F-OFDM while providing robustness against the nonlinearity of PA.

6.2 Future Work

There are some limitations in this thesis. Therefore, the following works can be extended in the future studies.

1. In this thesis, only point-to-point F-OFDM system was simulated. Hence, asynchronous transmission consisting of many sub-bands with different parameters such as modulation type, number of sub-carriers, CP length and filtering method can be also performance for real-life communication applications.

2. This study only considers AWGN as a wireless channel. Therefore, as a future work, the F-OFDM system over different types of channel, such as urban channel and marine channel, can be evaluated.

3. In this thesis, PAPR reducing technique and pre-distortion technique were applied in the system without integrating them optimally to achieve optimum performance between OOB and BER. Therefore, efficient combination of PAPR reducing technique and the pre-distortion technique suitable for F-OFDM system can be further studied.

Bibliography

[1] M. E. Charif. Evolution of mobile technology, 2015. URL https://www.linkedin.com/pulse/evolution-mobile-technology-mohamad-el-charif?ARTICLEId=5985483670654320640.

[2] Viracure. What's changed from 1G to 5G?, 2014. URL https://www.viracure.com/blog/from-1g-to-5g/.

[3] ITUR WP5D. IMT vision–framework and overall objectives of the future development of IMT for 2020 and beyond. Technical report, 2015.

[4] X. Zhang, M. Jia, L. Chen, J. Ma, and J. Qiu. Filtered-OFDM-enabler for flexible waveform in the 5th generation cellular networks. In *Global Communications Conference (GLOBECOM), 2015 IEEE*, pages 1–6. IEEE, 2015. doi: 10.1109/ICDSP.2014.6900754.

[5] P. Zhu. 5G enabling technologies–an unified adaptive software defined air interface, 2014. URL http://happyslide.net/doc/2572777/5g-enabling-technologies-an-unified-adaptive-software-def...

[6] J. Abdoli, M. Jia, and J. Ma. Filtered OFDM: A new waveform for future wireless systems. In *Signal Processing Advances in Wireless Communications (SPAWC), 2015 IEEE 16th International Workshop on*, pages 66–70. IEEE, 2015. doi: 10.1109/SPAWC.2015.7227001.

[7] A. V. Oppenheim. *Discrete-Time Signal Processing*. Pearson Education India, 1999.

[8] D. L. Jones. Parks McClellan FIR filter design, 2017. URL http://cnx.org/contents/0bb211fb-4a74-4efc-8a90-291cef969b75@3.

[9] J. G. Proakis and D. K. Manolakis. *Digital signal processing*. McGraw-Hill Toronto, Canada, 2006.

[10] L. Ding, G. T. Zhou, D. R. Morgan, Z. Ma, J. S. Kenney, J. Kim, and C. R. Giardina. A robust digital baseband predistorter constructed using memory polynomials. *IEEE Transactions on Communications*, 52(1):159–165, 2004. doi: 10.1109/TCOMM.2003.822188.

[11] L. Aladren, P. Garcia-Ducar, P. L. Carro, and J. de Mingo. Digital predistortion optimization using normalization gain adjustment in wideband systems. In *Microwave Conference (EuMC), 2013 European*, pages 420–423. IEEE, 2013. doi: 10.23919/EuMC.2013.6686681.

[12] National Instrument. Introduction and history of communications systems, 2016. URL `http://www.ni.com/white-paper/14797/en/`.

[13] M. Bellis. Alexander graham bell's photophone was an invention ahead of its time, 2017. URL `https://www.thoughtco.com/alexander-graham-bells-photophone-1992318`.

[14] Marconi Society. Guglielmo marconi, 2017. URL `http://www.seas.columbia.edu/marconi/history.html`.

[15] L. Kurup A. Gawade V. S. Jain, S. Jain. Overview on generations of network: 1G, 2G, 3G, 4G, 5G. *IOSR Journal of Electronics and Communication Engineering*, 9 (3), 2014. ISSN 2229-6093.

[16] M. R. Bhalla and A. V. Bhalla. Generations of mobile wireless technology: A survey. *International Journal of Computer Applications*, 5(4), 2010. doi: 10.1.1.206.5216.

[17] B. G. Gopal and P. G. Kuppusamy. A comparative study on 4G and 5G technology for wireless applications. *Journal of Electronics and Communication Engineering (IOSR-JECE)*, 10(6):67–72, 2015. ISSN 2278-2834. doi: 10.9790/2834-10636772.

[18] T. Hwang, C. Yang, G. Wu, S. Li, and G. Y. Li. OFDM and its wireless applications: A survey. *IEEE Transactions on Vehicular Technology*, 58(4):1673–1694, 2009. doi: 10.1109/TVT.2008.2004555.

[19] J. Li, K. Kearney, E. Bala, and R. Yang. A resource block based filtered OFDM scheme and performance comparison. In *Telecommunications (ICT), 2013 20th International Conference on*, pages 1–5. IEEE, 2013. doi: 10.1109/ICTEL.2013.6632084.

[20] 3GPP. Study on scenarios and requirements for next generation access technologies. Technical report, 2016.

[21] A. Farhang, M. M. Kakhki, and B. Farhang-Boroujeny. Wavelet-OFDM versus filtered-OFDM in power line communication systems. In *Telecommunications (IST), 2010 5th International Symposium on*, pages 691–694. IEEE, 2010. doi: 10.1109/ISTEL.2010.5734111.

[22] T. Wild, F. Schaich, and Y. Chen. 5G air interface design based on universal filtered (UF-) OFDM. In *Digital Signal Processing (DSP), 2014 19th International Conference on*, pages 699–704. IEEE, 2014. doi: 10.1109/ICDSP.2014.6900754.

[23] H. Lin. Flexible configured OFDM for 5G air interface. *IEEE Access*, 3:1861–1870, 2015. doi: 10.1109/ACCESS.2015.2480749.

[24] X. Cheng, Y. He, B. Ge, and C. He. A filtered OFDM using FIR filter based on window function method. In *Vehicular Technology Conference (VTC Spring), 2016 IEEE 83rd*, pages 1–5. IEEE, 2016. doi: 10.1109/VTCSpring.2016.7504065.

[25] M. M. Mowla and S. M. M. Hasan. Performance improvement of PAPR reduction for OFDM signal in lte system. *International Journal of Wireless & Mobile Networks (IJWMN)*, 5(4):35–47, 2013. ISSN 0975-3834. doi: 10.5121/ijwmn.2013.5403.

[26] I. C. Sezgin. Different digital predistortion techniques for power amplifier linearization. Master's thesis, LUND University, 2016.

[27] L. Ding. *Digital predistortion of power amplifiers for wireless applications*. PhD thesis, Georgia Institute of Technology, 2004.

[28] Y. C. Wang and Z. Q. Luo. Optimized iterative clipping and filtering for PAPR reduction of OFDM signals. *IEEE Transactions on Communications*, 59(1):33–37, January 2011. doi: 10.1109/TCOMM.2010.102910.090040.

[29] B. Farhang-Boroujeny. OFDM versus filter bank multicarrier. *IEEE Signal Processing Magazine*, 28(3):92–112, 2011. doi: 10.1109/MSP.2011.940267.

[30] M. Faulkner. The effect of filtering on the performance of OFDM systems. *IEEE Transactions on Vehicular Technology*, 49(5):1877–1884, 2000. doi: 10.1109/25.892590.

[31] V. Vakilian, T. Wild, F. Schaich, S. T. Brink, and J. F. Frigon. Universal-filtered multi-carrier technique for wireless systems beyond LTE. In *Globecom Workshops (GC Wkshps), 2013 IEEE*, pages 223–228. IEEE, 2013. doi: 10.1109/GLOCOMW.2013.6824990.

[32] D. Wu, X. Zhang, J. Qiu, L. Gu, Y. Saito, A. Benjebbour, and Y. Kishiyama. A field trial of f-OFDM toward 5G. In *Globecom Workshops (GC Wkshps), 2016 IEEE*, pages 1–6. IEEE, 2016. doi: 10.1109/GLOCOMW.2016.7848810.

[33] P. Guan, D. Wu, T. Tian, J. Zhou, X. Zhang, L. Gu, A. Benjebbour, M. Iwabuchi, and Y. Kishiyama. 5G field trials-OFDM-based waveforms and mixed numerologies. *IEEE Journal on Selected Areas in Communications*, 2017. doi: 10.1109/JSAC.2017.2687718.

[34] J. Vuolevi and T. Rahkonen. *Distortion in RF power amplifiers*. Artech house, 2003.

[35] Mathworks. gausswin, 2017. URL `https://www.mathworks.com/help/signal/ref/gausswin.html`.

[36] A. Antoniou. *Digital Filters, Analysis, Design, and Applications*. McGraw-Hill, 2000.

[37] A. A. M. Saleh. Frequency-independent and frequency-dependent nonlinear models of TWT amplifiers. *IEEE Transactions on Communications*, 29(11):1715–1720, 1981. doi: 10.1109/TCOM.1981.1094911.

[38] H. W. Kang, Y. S. Cho, and D. H. Youn. On compensating nonlinear distortions of an OFDM system using an efficient adaptive predistorter. *IEEE Transactions on Communications*, 47(4):522–526, 1999. doi: 10.1109/26.764925.

[39] K. Narendra and P. Gallman. An iterative method for the identification of nonlinear systems using a Hammerstein model. *IEEE Transactions on Automatic Control*, 11 (3):546–550, 1966. doi: 10.1109/TAC.1966.1098387.

[40] L. Gan and E. Abd-Elrady. Digital predistortion of memory polynomial systems using direct and indirect learning architectures. In *Proceedings of the IASTED International Conference*, volume 654, page 802, 2009.

[41] S. M. Kay. *Fundamentals of Statistical Signal Processing, Volume I: Estimation Theory*. Prentice Hall, 1993.

[42] A. Zhu, P. J. Draxler, J. J. Yan, T. J. Brazil, D. F. Kimball, and P. M. Asbeck. Open-loop digital predistorter for rf power amplifiers using dynamic deviation reduction-based volterra series. *IEEE Transactions on Microwave Theory and Techniques*, 56 (7):1524–1534, 2008. doi: 10.1109/TMTT.2008.925211.

[43] K. J. Muhonen, M. Kavehrad, and R. Krishnamoorthy. Look-up table techniques for adaptive digital predistortion: A development and comparison. *IEEE Transactions on Vehicular Technology*, 49(5):1995–2002, 2000. doi: 10.1109/25.892601.

[44] H. Durney. *Adaptive pre-distortion for nonlinear high power amplifiers in OFDM systems*. PhD thesis, Polytechnic University of Catalonia, 2004.

[45] A. Gangwar and M. Bhardwaj. An overview: Peak to average power ratio in OFDM system & its effect. *International Journal of Communication and Computer Technologies (IJCCTS)*, 1(2):22–25, 2012. ISSN 2278-9723.

[46] S. Boyd. CVX: Matlab software for disciplined convex programming, 2016. URL `http://cvxr.com/cvx/`.

[47] M. S. Lobo, L. Vandenberghe, S. Boyd, and H. Lebret. Applications of second-order cone programming. *Linear algebra and its applications*, 284(1-3):193–228, 1998.

[48] W. H. Chin, Z. Fan, and R. Haines. Emerging technologies and research challenges for 5G wireless networks. *IEEE Wireless Communications*, 21(2):106–112, 2014. doi: 10.1109/MWC.2014.6812298.

[49] J. C. M. Mota, C. A. R. Fernandes, and G. Favier. Modeling of OFDM systems with memory polynomial power amplifiers. In *XXIX Simpósio Brasileiro de Telecomunicações (SBrT)*, 2011.

[50] X. Li and L. J. Cimini. Effects of clipping and filtering on the performance of OFDM. In *Vehicular Technology Conference, 1997, IEEE 47th*, volume 3, pages 1634–1638. IEEE, 1997. doi: 10.1109/4234.673657.